UNIVERSITY OF CAMBRIDGE

Department of Engineering

Sinkhole Formation: can a comparison with tunneling illuminate the process?

Author Name: Tobias Möller

Supervisor: Dr C.N. Abadie

Date: 26/05/2020

I hereby declare that, except where specifically indicated, the work submitted herin is my own original work.

Signed ________________ *date* 26/05/2020

Abstract

Sinkholes can cause significant damage to existing infrastructure when forming and collapsing. An early warning system would enable remedial action to be undertaken before the eventual collapse of the sinkhole, to protect infrastructure and potentially save lives.

1g laboratory testing was performed on a 2D plane strain trapdoor rig to simulate the sinkhole formation process. Fibre optic cables were used to collect data in order to explore their potential as an early warning system. The behaviour of the cable is known to be governed by the interface friction between the fibre and the surrounding soil, and also the pretension due to the laying method used. Different techniques for laying fibre optic cables were explored and it showed that increasing the interface roughness of the fibre is beneficial. This is achieved by coating the fibre in sand before laying. Furthermore, introducing slack into the fibre in the vicinity of ground deformations improves the ability of the fibre to follow the deformations.

The fibre optic data from the 1g tests contained a signature strain profile which could be used to identify sinkholes. In order for fibre optic cables to be used for an early warning system it is important to understand the data outputted by the fibre. The fibre data was compared with PIV data obtained simultaneously, demonstrating that there is significant slipping between the fibre and the surrounding soil. Nevertheless, the fibre strain profile is comparable with the dominant strain profile obtained from the PIV data. This dominant strain profile is the horizontal profile in the soil. The magnitude of the fibre profile is considerably less due to the greater rigidity of the fibre along its length, when compared to the surrounding soil. The fibre profile width is nonetheless greater than the PIV profile which is likely due to slipping between the fibre and the soil.

There are significant similarities between the ground behaviour in sinkhole formation and in tunnelling. Accordingly, a 1g test was performed on a miniature TBM rig to enable a comparison of the two tests. Fibre optic data was collected from the TBM rig, allowing further analysis of the fibre data. It was demonstrated that it is possible to determine whether the soil is settling or heaving from the fibre optic data, and also when a transition between the two behaviours occurs. In addition, the fibre data indicates the direction of rotation of the cutterhead. Finally, both in the transverse direction and the longitudinal direction the fibre data is dominated by the horizontal strains as experienced by the soil.

A comparison between the plane strain trapdoor rig and tunnelling was performed by comparing the obtained data with literature. It was demonstrated that the trends present in the data closely matched those found in existing literature on other rigs and also using FEM.

The fibre optic data was directly compared across the two tests, showing that the obtained profiles were very similar in both shape and magnitude. The TBM fibre profile was found to be wider than the trapdoor profile, aligning with the fact that the TBM rig involves more horizontal movement due to the cylindrical nature of the tunnel and the rotation of the cutterhead, whereas the trapdoor rig is dominated by a steep chimney mechanism.

Analysis of the fibre optic data obtained in the trapdoor rig thus shows the potential of using fibre optic cables to predict sinkholes. The data contains a signature strain profile which is readily recognisable and indicates the centre of the sinkhole. Combined with another detection technique, such as GPR, fibre optic cables could be successfully used as an early warning system for sinkholes. The laying technique plays an important role and increasing the interface roughness of the fibre is beneficial. Further research is required to enable accurate determination of the size and depth of a sinkhole based upon the fibre optic data alone.

Tests in the TBM rig further confirm the usefulness of the fibre data, and the two tests combined allow initial conclusions to be formed about the behaviour of the fibre. A comparison between the trapdoor rig and existing literature highlights strong similarities between the trapdoor rig and tunnelling. This is further emphasised, upon comparison of the fibre data obtained in both tests. This suggests that similar analysis techniques can be applied to both processes and similar experimental methodologies can be used.

Table of Contents

1 Introduction

1.1 Context

A sinkhole/doline is a depression formed due to collapse of the surface layer, usually caused by the dissolution of carbonate rocks at depth. Karst terrain – a composition of soluble rocks such as limestone, dolomites, and evaporites such as gypsum or chalk – are particularly susceptible to sinkhole formation. The collapse of existing, underground, manmade structures such as old mine shafts, can also facilitate the formation of sinkholes.

Sinkholes have the potential to cause considerable damage to existing infrastructure on the surface, that could potentially lead to loss of life. At present there is no known, effective method for predicting and locating sinkholes before they have reached the surface, and hence there is a drive to develop an early warning and detection system for sinkholes.

In the UK, the proposed High Speed 2 (HS2) development, aimed at expanding the high-speed railway infrastructure, follows a route crossing over large areas of terrain which are known to

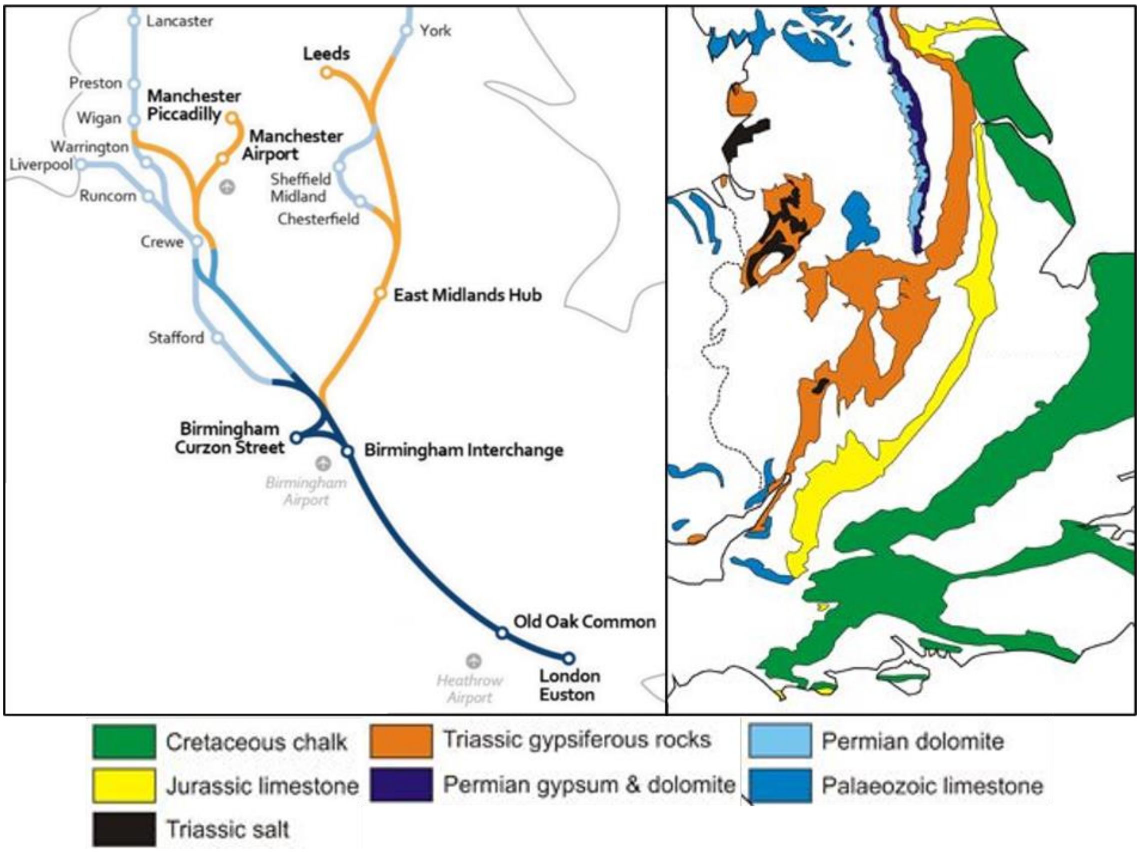

Figure 1: A map of the intended route for HS2 (left) (BBC); and a map showing terrain susceptible to sinkhole formation (right) (British Geological Survey).

be susceptible to sinkhole formation (Figure 1). Accordingly, the CSIC is working on developing an early warning system for sinkholes, to help protect HS2 from the damage that sinkholes can cause to railways. This project forms a part of the development process for this system. The intention is to use fibre optic cables to monitor subsurface ground movements and deformations to locate and predict sinkholes before they cause damage, allowing remedial action to be taken.

1.2 Project Contribution and Objectives

This project is concerned with performing experiments at 1g, to explore the viability of an early warning system and compare the sinkhole formation process with tunnelling.

The project is split into three main objectives:

1. *Laying of fibre optic cables* – The aim is to explore how to use distributed fibre optic sensing (DFOS) techniques for accurate data acquisition in 1g laboratory experiments. Two main effects are explored. Firstly, the coupling between the fibre optic cable and the surrounding sand and secondly, the residual tension due to the fibre laying process. DFOS enables data collection at high spatial resolution and hence could enable detailed monitoring of sand behaviour, making it very applicable to 1g geotechnical testing. Accordingly, it is important to improve the understanding of how DFOS is affected by a range of factors, such as the residual tension and coupling with the surrounding soil.
2. *Making sense of the data collected from DFOS during the formation of a sinkhole* – This can be explored by comparing the data with the geomechanics of sinkhole formation observed in controlled conditions. This is achieved by using particle image velocimetry (PIV). DFOS has not previously been used for monitoring sinkhole formation, with the exception of the work from Della Ragione (2020). Hence, analysing the fibre optic data demonstrates that DFOS is applicable to sinkhole monitoring and provides evidence that its use for real-life monitoring can be feasible.
3. *Comparing the formation of sinkholes to the tunnelling process* – This is a comparison which has not previously been explored. However, the settlement and strain profiles obtained in sinkhole formation and tunnelling show similarities, and accordingly it is possible to improve our understanding of sinkholes, by drawing on knowledge of tunnelling ground deformations.

2 Literature Review

2.1 Sinkholes

2.1.1 Sinkhole Formation

Sinkholes mainly occur in Karst terrain – a composition of materials formed by the dissolution of soluble rocks, such as limestone, dolomite, and gypsum (Rawal, 2016). Karst terrains develop a high level of permeability as water travels through and dissolves the terrain (Tien, 1996). Sinkholes form due to a variety of processes. The most dangerous of these is the collapse doline (Figure 2) as they form rapidly and with little to no prior warning. Accordingly, it is the formation of collapse dolines in particular which require further understanding and careful monitoring, in order to prevent or minimise damage to infrastructure and potentially danger to life. Chang and Hanssen (2014) found that collapse sinkholes can develop over extended periods of time, with measurable ground deformation developing over the course of several days, weeks or even years before the eventual collapse of the sinkhole. This gives credence to the development of an early warning system.

Most collapse sinkholes form as a result of lowering the water table, which leads to an increase in the effective stress above a cavity, causing the overburden pressure to increase on the cavity roof, and this leads to collapse (Jennings *et al.*, 1965). Cohesion is therefore an important factor in determining the strength of a cavern roof. Where cohesion is not present the deciding factor is the arching mechanism which controls the transmission of stresses above the cavity. There are a number of conditions which must be fulfilled in order for a collapse sinkhole to form (Jennings *et al.*, 1965):

- Adjacent, rigid material is required to form abutments for the void.
- A condition of arching must develop in the residuum.

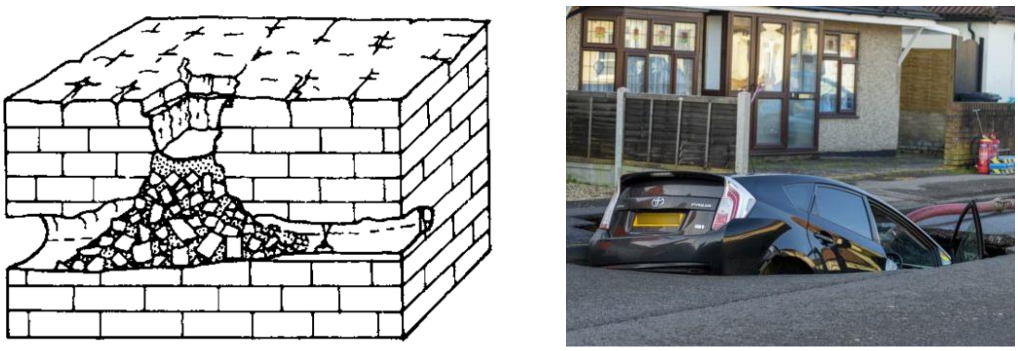

Figure 2: Collapse doline (left) (J. N. Jennings, 1971); and a sinkhole in Essex (right) (Ricci Fothergill).

- A void must form below the arch.
- A reservoir must exist below the arch to accept the material from the sinkhole.
- Some disturbance must occur to cause roof collapse.

Arching in soils is caused by relative displacement. This movement is opposed by shear stresses in the soil, leading to a reduction in the stress level in soil regions with large movement, and an increase in stationary soil regions. This causes the soil to arch over the moving soil (Terzaghi, 1936).

2.1.2 Physical Modelling

A range of physical models have been used to simulate sinkholes. Table 1 provides a summary of the different physical models used to date for research purposes, and their advantages and disadvantages.

Alrowaimi, Yun and Chopra (2015) discovered that before a sinkhole collapses a distinguishable groundwater cone of depression forms around the sinkhole. This cone steepens over time as the sinkhole develops. The cone can be used to indicate the location of a sinkhole before collapse occurs. However, in practice, this requires accurate knowledge of where sinkholes will form and a large number of groundwater monitoring wells, which is often not possible. Labuschagne *et al.*, 2019 observed that the maximum strains occurred before the maximum surface settlements were visible, suggesting another potential method for locating sinkholes.

Table 1: A summary of the different physical models used to simulate sinkholes.

Model	g-level	Advantages	Disadvantages
Hole or crack in the base of a container.	1g	Allows for easy exploration of groundwater and other patterns in the vicinity of sinkholes.	Not possible to simulate the formation process.
Deflation of a water filled balloon or similar.	1g or ng	Allows simulation of a 3D spherical sinkhole, which more accurately depicts the shape of real sinkholes.	Hard to extract data for the sub-soil movements.
Hole or fissure within the model where sinkhole formation is initiated by a change in hydraulic head.	1g	Allows the effect of hydraulic head on the formation process to be explored.	Difficult to control the speed and extent of sinkhole formation.
2D plain strain trapdoor model.	1g or ng	Allows the formation process to be explored in detail, with greater control over the size of sinkhole.	Does not simulate accurately the shape of a sinkhole.

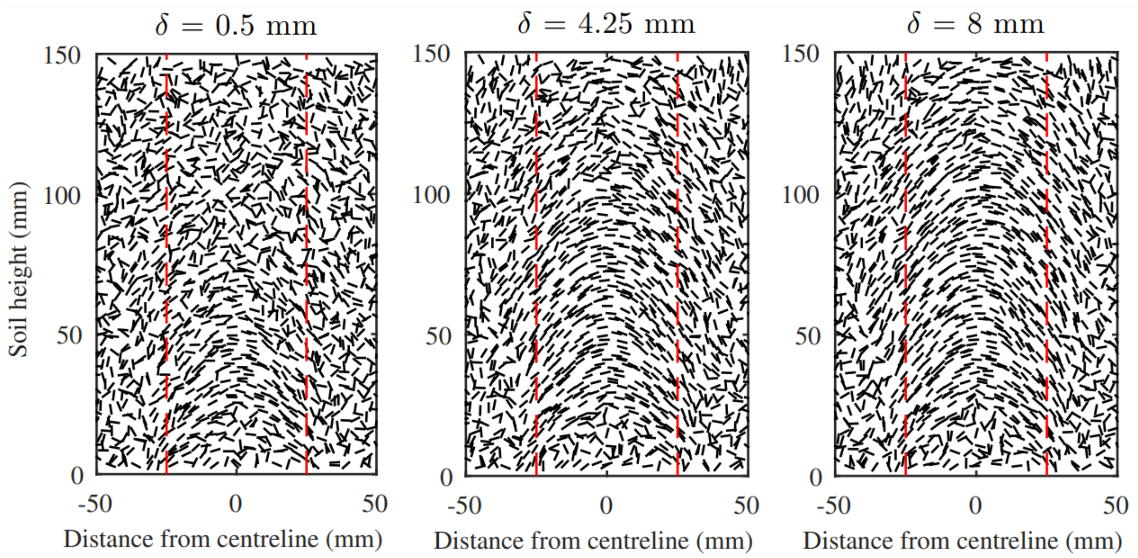

Figure 3: Rotation of major principal strains, at different displacements of the trapdoor, showing the formation of a soil arch (da Silva, 2017).

The arching effect leads to a drop in stress at the top of the cavity. These stresses are transferred to the corners, leading to an increase in stress at these locations (Soliman *et al.*, 2018). The rotation of principal strains allows the presence of stress redistributions in the soil to be visualised, with a continuous arc of major principal strains forming across the void (Figure 3) (da Silva, 2017).

Jacobsz (2015) demonstrated that movement within the trapdoor models occurred almost entirely along distinct shear bands. The sand immediately above the trapdoor begins to dilate, and symmetric shear surfaces propagate from the trapdoor edges to form a triangular failure wedge (Figure 4). As the trapdoor moves further the shear surface becomes less symmetric, although more symmetry is present in larger trapdoor models (Jacobsz, 2015). The slope and

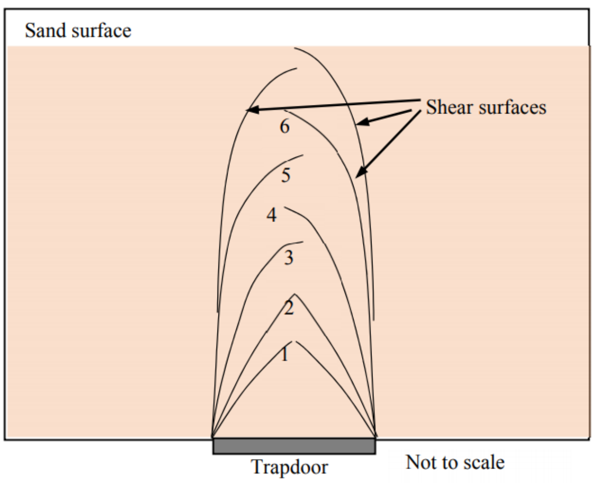

Figure 4: The shear surface formation process as the trapdoor is lowered (Jacobsz, 2015).

curvature of the shear surface depends on the dilation characteristics of the sand (Costa *et al.*, 2009); determined by the soil density and its confinement. After the initial symmetrical behaviour, shear zone development alternates between the left- and right-hand sides of the trapdoor. The angle between the vertical and the tangent was found to equal the soil dilatancy angle. The density of the soil decreases as the trapdoor moves and hence the soil dilatancy decreases, causing the failure surface to tend towards the vertical in several discontinuous jumps (Costa *et al.*, 2009).

As the advancing zone propagates the zone of influence narrows, initially leading to a triangular shape which forms at the point of maximum arching (da Silva, 2017). This develops into a parabolic shape (Figure 5). The sides of the shaft of sand moving downwards approach the vertical as the advancing zone reaches the surface (Iglesia, Einstein and Whitman, 2014), with a width similar to the width of the trapdoor. There is potential for the sides to begin to slump inwards at the surface, causing the shaft to take on a funnel shape (Jacobsz, 2015). Shallow, wide surface settlements were observed at greater heights above the trapdoor, with deeper narrow profiles further down (da Silva, 2017). Of particular interest is da Silva's (2017) UNRNF-2 test, as this was performed with the same cover to diameter ratio as the tests in this thesis. Accordingly, data from this project is compared to UNRNF-2 in order to explore the relationship between 1g and centrifuge testing.

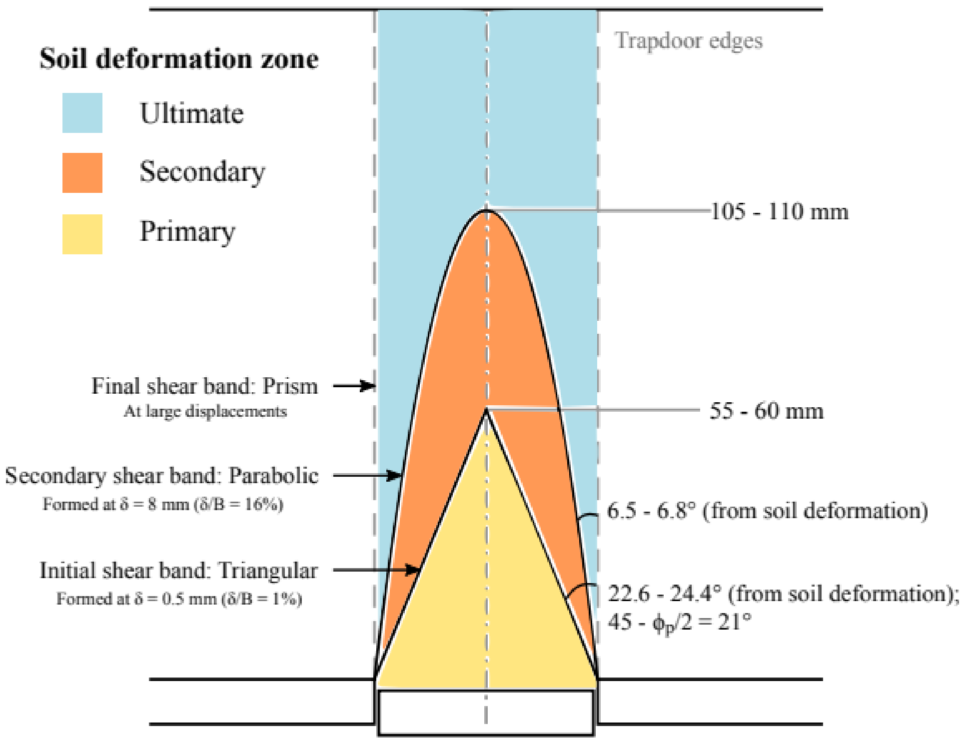

Figure 5: Shear band development throughout the test (da Silva, 2017).

Costa *et al.* (2009) proved that the higher the stress level the more well defined the failure zones are, and the magnitude of surface settlements is greatly influenced by the relative density, with loose soils leading to greater surface settlements.

Al-Naddaf *et al.* (2017) found that the presence of a geosynthetic helps to transfer more loads onto the supports thereby preventing the soil arch from deteriorating under self-weight.

2.1.3 Numerical Modelling

A range of numerical models have been used to simulate the sinkhole formation process. One example of such a model is the conceptual FLAC (a two-dimensional, explicit finite difference program) model created by Rawal (2016). In this study different parameters in the sinkhole formation process were varied and the effects of this were simulated. The results demonstrated that increasing the diameter of a cavity increases the vertical deformation and the vertical stress. Increasing the overburden pressure led to an increase of the vertical deformation. Different shapes were also explored, and a square cavity was found to deform more than a circular one. The model showed that lowering the water table increased the vertical stresses and thereby increased the vertical deformations. Finally, the effect of cohesion was studied, and it was observed that greater cohesion leads to less vertical deformation.

2.1.4 Monitoring

There are a variety of different monitoring techniques used to study sinkholes, compared in Table 2. The most promising of these are time domain reflectometry (TDR), differential synthetic aperture radar interferometry (DInSAR) and DFOS. DInSAR is able to cover extremely large areas but relies on the satellite's repeat-orbit cycle for its temporal frequency. Both TDR and DFOS are particularly well suited to monitoring infrastructure such as roads or

Table 2: A summary of the different techniques used to monitor sinkholes.

Technique	Can locate collapse abnormalities	Temporal Frequency	Area coverage	Resolution
Ground penetrating radar (GPR)	✓	Very low	Low	Low
Monitor water or air pressure changes	✓	High	Very low	n/a
TDR	✓	Very High	Medium	High
DInSAR	✓	Low	Very high	Medium
DFOS	✓	Very High	Medium	Very high

railways, as they can be laid in continuous lines. However, they rely on the interface between the fibre and the soil, which is one of the barriers to their adoption.

Zhang, Zhu and Shi (2016) found that the overburden pressure can effectively tighten the fibre-soil interface, thereby extending the measurement range of the optical fibre. Peak and residual interfacial shear strengths increase with soil density, indicating that increasing the soil density enhances the fibre-soil interface. The tension in the fibre increased with displacement up to a given maximum, beyond which point the tension remained fairly constant. The strain initiates at the loading point and then propagates towards the ends of the fibre.

Della Ragione (2020) worked on monitoring sinkhole formation using DFOS, as part of a collaboration with CSIC and the project presented in this report, performing preliminary tests using the same experimental setup and comparing the results to finite element models with Plaxis 3D. The numerical results showed that horizontal soil movements are influenced by the presence of the cables, and that the strain within the fibres is governed by the horizontal movement of the soil. The research presented in this report aims to continue and further the understanding of monitoring sinkhole formation using DFOS.

Summary

The causes of sinkhole formation have been explored using a variety of laboratory tests. This has informed the research into available monitoring techniques and several promising options have been discovered. However, at present, none of these are readily adopted due to various barriers, such as the interface between optical fibres and the soil. This project forms a part of the necessary further research into resolving these barriers.

2.2 Tunnelling

2.2.1 Ground Behaviour

Tunnelling is a major aspect of geotechnical engineering. When tunnelling is undertaken it is important to predict the ground surface movements as these will impact existing surface infrastructure. The prediction of these movements can be split into two phases (Glossop, 1978): prediction of the volume of ground lost during the course of tunnelling and determining how and to what extent this volume loss is transmitted to the surface.

The main causes of ground losses are face relaxation, radial take as the soil tightens around the permanent liner behind the shield, and ovalling of the excavation due to steering manoeuvres (Selby, 1999). The settlements on the surface are directly proportional to these ground losses,

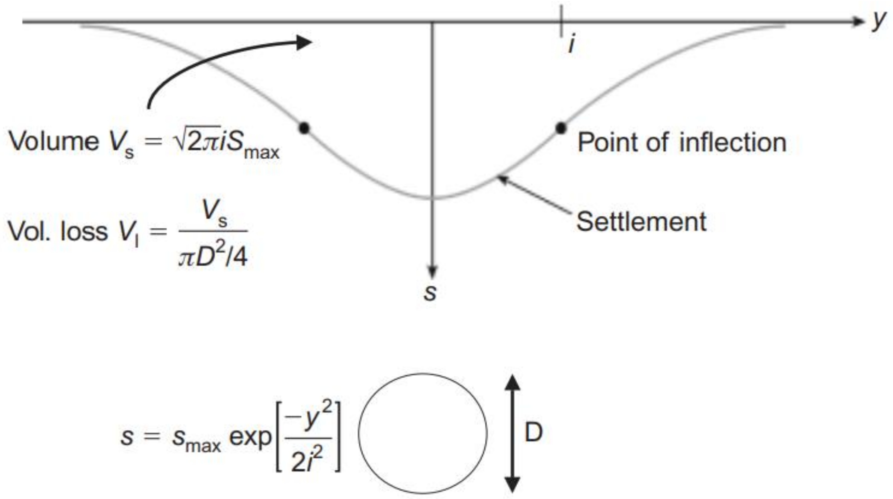

Figure 6: The gaussian distribution (Mair, 2008).

which are a function of the soil type and the tunnelling method used. Volume losses in granular soils are typically larger, poorly controlled, and unpredictable (Selby, 1999).

Mair (2008) demonstrated that for undrained clay the settlement profile is well fitted by a gaussian curve (Figure 6). This curve is defined by the maximum settlement, S_{max} and the horizontal distance between the inflection point and the tunnel axis, i_x. O'Reilly and New (1982) proved that the value of i_x varies with the depth of the tunnel:

$$i_x = Kz_0 \tag{1}$$

where $K = 0.2 - 0.45$ for granular materials (Fargnoli, Boldini and Amorosi, 2013) and z_0 is the depth of the tunnel centreline. Furthermore, for low cover-to-diameter ratios (C/D), i_x is a function of the tunnel diameter, D:

$$\left(\frac{i_x}{D/2}\right) = \left(\frac{C}{D}\right)^{0.7} \tag{2}$$

The volume loss parameter, V_L, can be calculated from $V_L = V_S/A_t \times 100\%$ where A_t is the area of the tunnel face and V_S is the volume of the surface settlement trough per unit length of the tunnel. V_S may be calculated as follows (Fargnoli, Boldini and Amorosi, 2013):

$$V_S = \int_{-\infty}^{+\infty} S_v(x)\, dx = \sqrt{2\pi} i_x S_{max} \tag{3}$$

where x is the horizontal distance from the tunnel centreline and S_v is the settlement at a given point. As the transverse settlement trough is well approximated by a gaussian curve (Figure 6), then the longitudinal settlement profile should be well described by a cumulative gaussian probability curve with the following expression (Fargnoli, Boldini and Amorosi, 2013):

$$S_v(y)_{x=0} = S_{max}\phi\left(\frac{y}{i_y}\right) \tag{4}$$

where $\phi\left(\frac{y}{i_y}\right)$ is given by:

$$\phi\left(\frac{y}{i_y}\right) = \frac{1}{i_y\sqrt{2\pi}}\int_{-\infty}^{y} exp\left(-\frac{y^2}{2i_y^2}\right)dy \tag{5}$$

where y is the longitudinal distance ahead of the tunnel face and i_y is a length parameter.

However, for tunnels in sand the gaussian curve does not provide a good fit for the settlement profile (Vorster *et al.*, 2005). For sand, the volume of the soil is not constrained, allowing shearing to cause contraction and dilation (Marshall *et al.*, 2012). This leads to the volume of the settlement trough varying with depth. Accordingly, an assessment of volume loss based on surface measurements will not provide an entirely accurate measurement of subsurface volume loss.

Vorster *et al.* (2005) carried out centrifuge experiments and found that a modified gaussian distribution provided a good fit to the soil settlement profile obtained in sands:

$$S_v = \frac{n}{(n-1) + exp\left[\alpha\left(\frac{x}{i_x}\right)^2\right]}S_{max} \tag{6}$$

where α is a parameter to ensure that i_x remains the distance to the inflection point. n is given by the following equation:

$$n = e^{\alpha}\frac{2\alpha - 1}{2\alpha + 1} + 1 \tag{7}$$

According to Klar, Dromy and Linker (2014), a 3D gaussian model takes account of both the horizontal distance from the tunnel centreline and the longitudinal distance ahead of the tunnel face to predict the settlement at a given point in 3D space:

$$S_v = \frac{S_{max}}{2} \exp\left(-\frac{1}{2}\frac{x^2}{i_x^2}\right)\left(1 - erf\left(\frac{y}{\sqrt{2}i_y}\right)\right) \tag{8}$$

where $erf(g)$ is the error function:

$$erf(g) = \frac{2}{\sqrt{\pi}}\int_0^g e^{-t^2}dt \tag{9}$$

2.2.2 Physical Modelling

A range of physical models have been used to simulate tunnelling, including a plane-strain trapdoor model as described in Section 2.1.2. The trapdoor model is considered to be an approximate method to simulate ground response to tunnelling and it facilitates the evaluation of surface settlements and corresponding earth pressures on tunnel linings (Meguid *et al.*, 2008). Other models include placing soil around pre-installed tubes and controlling the supporting pressure to simulate near face stability; pressurised air bags which are deflated to simulate volume loss; and miniature tunnel boring machines (TBMs).

Marshall *et al.* (2012) showed that the value of i_x decreases with depth and volume loss. They also discovered that the key geometric and tunnelling parameters which govern the settlement trough shape in sand are relative density, cover to diameter ratio and volume loss. At low tunnel volume losses, there is little difference between the soil and tunnel volume loss so very little volumetric strain occurs. At higher tunnel volume losses, the overall effect of soil dilation is apparent as the soil volume loss eventually becomes less than the tunnel volume loss. As the tunnel volume increases the trough width decreases and the same occurs as the depth increases or the cover to diameter ratio decreases.

2.2.3 Monitoring using DFOS

Fibre optic cables have only recently been used to measure ground deformations for tunnelling applications and this concept was explored by Klar, Dromy and Linker (2014). Monitoring tunnelling settlements using fibre optic cables is a soil-fibre interaction problem in which the rigidity of the fibre may alter the resultant deformation. However, it has been demonstrated that the fibre practically follows the soil due to its low rigidity.

According to Klar, Dromy and Linker (2014) there are two main equivalent approaches for relating ground displacements to the expected longitudinal strain in the fibre. One is by evaluating the longitudinal displacement along the fibre and differentiating this with distance, the other is through transformation of the soil strain tensor.

The expression for the fibre strain, c_f, for the case when the tunnel axis is transverse to the fibre, may be written as (Klar, Dromy and Linker, 2014):

$$c_f = \frac{nS_{max}}{2z}\frac{x_f^2 - i_x^2}{i_x^2} exp\left(-\frac{1}{2}\frac{x_f^2}{i_x^2}\right)\left(1 - erf\left(\frac{L}{\sqrt{2}i_y}\right)\right) \quad (10)$$

where z is the height between the tunnel centreline and the point of interest.

2.2.4 Knowledge Transfer from Tunnelling to Sinkhole Formation

Costa *et al.* (2009) proved that the settlements experienced in sinkhole formation can be characterised by a gaussian fit in the same way that tunnelling settlements are (Section 2.2.1). This suggests that not only the ground behaviour, but also the strain profiles across the two processes are similar.

Summary

Ground behaviour in tunnelling has been studied and a variety of laboratory tests have been performed. These have shown that tunnelling exhibits similarities with the sinkhole formation process. However, these similarities have not been quantified beyond noting that ground deformations adopt a gaussian distribution in both. This project aims to further explore and quantify these similarities.

3 Experimental Methods

Tests were performed on the lab floor using a plane strain trapdoor model at 1g in order to explore the sinkhole formation process using DFOS. This was compared to a test conducted using a miniature TBM allowing the similarities between the two rigs to be explored.

3.1 Plane Strain Trapdoor

A 2D plane strain box with a Perspex window was used to simulate the formation of sinkholes by lowering a trapdoor using a hydraulic cylinder. The displacement of the trapdoor was recorded using linear variable differential transformers (LVDTs) mounted below the trapdoor. The box has internal dimensions of 790 x 200 x 560 mm and the trapdoor has a width of 100 mm (Figure 7). With the false floor the available soil height is approximately 370 mm. The Perspex window is polished, and the internal walls of the box are plated with polished hard chrome to minimise friction. This is the same rig as was used by da Silva (2017) and Della Ragione (2020).

3.1.1 PIV

The Perspex window of the plane strain trapdoor box allows PIV to be used in order to measure the soil displacements. This requires a camera setup for recording images throughout the test (Figure 8(a)). The geoPIV-RG version of the PIV software was used (Stanier *et al.*, 2015). This technique uses a sequence of photographs, taken during the test with a pair of Canon Powershot G10 cameras, to track the movement of the soil. This is achieved by tracking a grid of soil patches from one image to the next by looking for similarity in contrast patterns. In order to convert the obtained soil displacements in pixel space, into millimetre displacements, a

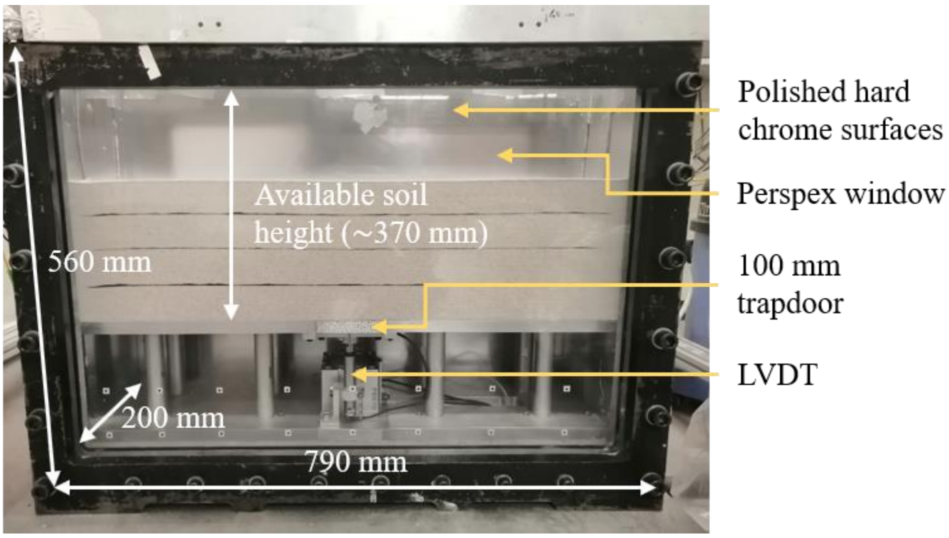

Figure 7: The plane strain trapdoor box.

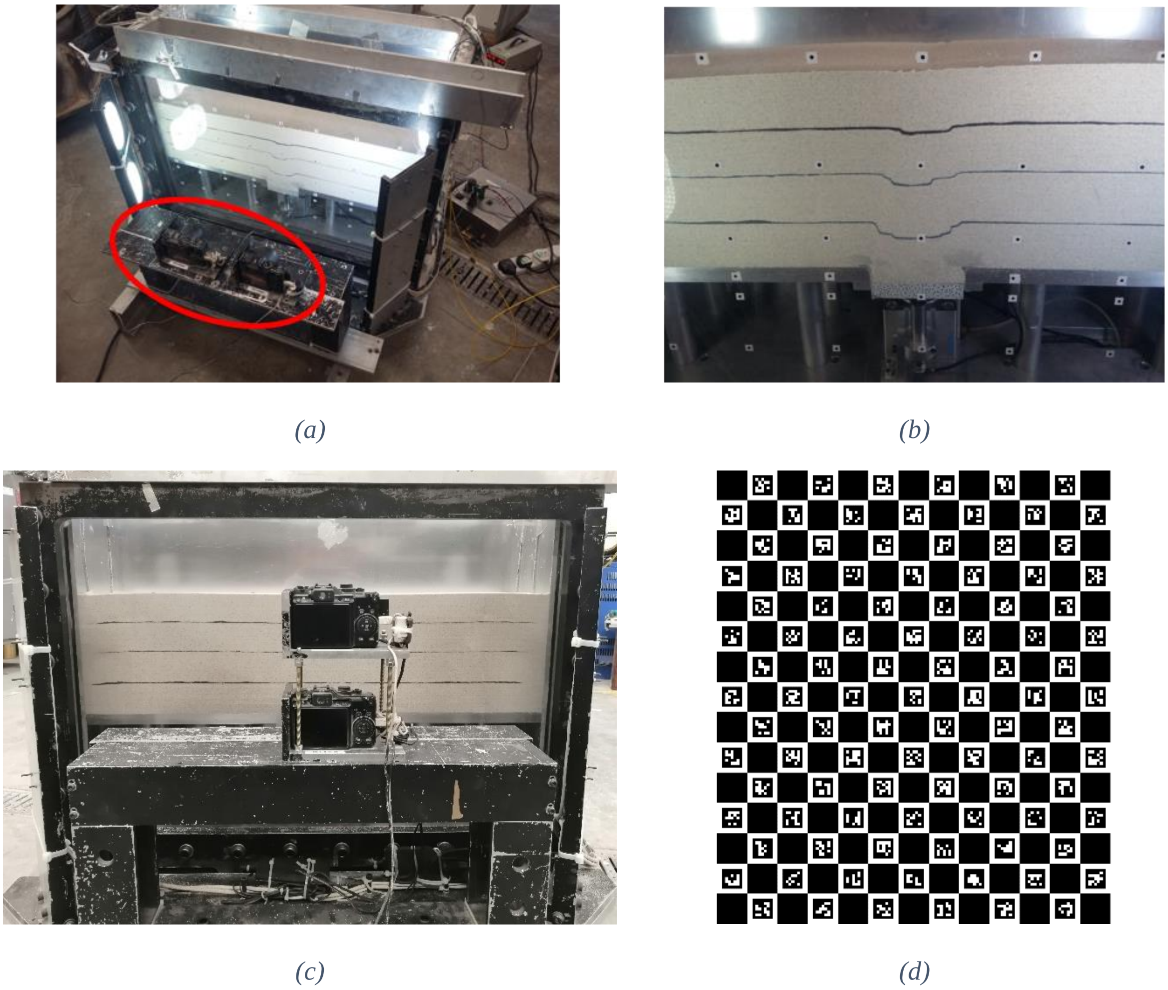

Figure 8: Evolution of PIV test set-up – initial set-up (a); control markers used for PIV calibration (b); improved camera setup for the PIV system (c); and CharuCo board (d).

calibration procedure is required. A series of control markers (Figure 8(b)) are attached to the Perspex window and their known locations are used to calibrate the cameras. This procedure corrects the obtained data for distortion and rotation and enables the required coordinate conversion.

The PIV data obtained in the first test was too noisy, and accordingly the cameras were moved closer to the rig in order to improve the quality of the data. However, in the second test this issue was still not remedied (Figure 9), and hence for the third test the cameras were moved even closer to the rig, at which point it became necessary to stack two cameras on top of each other to cover the entire height of the sample (Figure 8(c)). The data obtained in the third test was of a considerably higher quality than the data from the first two tests (e.g. Figure 9) and enabled more detailed analysis of the geomechanics of sinkhole formation (Section 4.4).

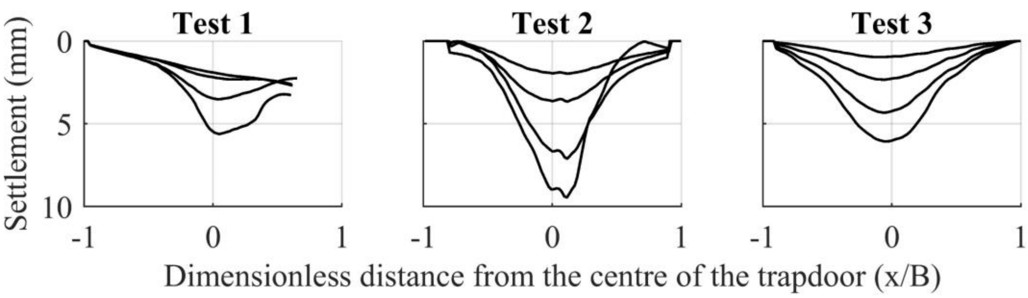

Figure 9: Settlements obtained from the PIV data for the top layer (see Section 3.1.2), for trapdoor displacements of 2, 6, 12 and 16 mm, for the three tests.

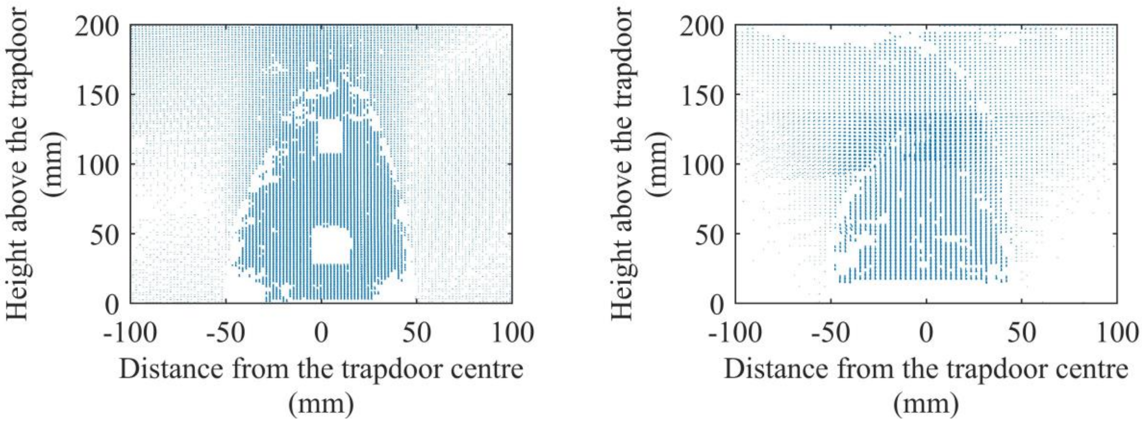

(a) *(b)*

Figure 10: Quiver plots of soil displacements from Test 2 (a); and Test 3 (b).

It was also observed that the control markers led to data losses in the first two tests, as shown in Figure 10(a), and so a different calibration technique was used for the third test which does not require the use of control markers. A CharuCo board (Figure 8(d)) was used to calibrate the cameras prior to running the third test. Due to the removal of the control markers the data losses were remedied (Figure 10(b)).

3.1.2 DFOS

Fibre optic cables were placed inside the body of the soil to explore the strain profiles obtained and allow comparison of these to the PIV data. 2 mm diameter black fibre optic cables were used, with a 9 μm silica glass core. The Young's modulus of the fibres is 200 MPa. These fibres

Figure 11: Luna ODiSI 6100 optical distributed sensor interrogator.

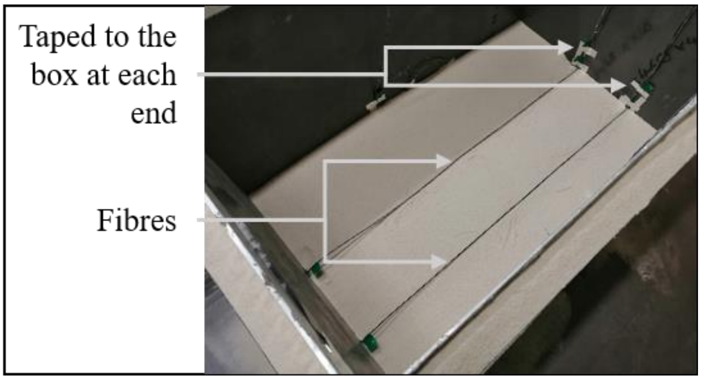

Figure 12: Fibres running across the box and taped at each end.

Figure 13: Fibre having been coated in glue and rolled in sand.

were connected to the Luna ODiSI 6100 DFOS analyser (Figure 11) which enables measurement of the Rayleigh back-scattered light in optical fibres (Kechavarzi, 2016). This analyser has a particularly small spatial resolution (2.6 mm were used throughout this project) making it suitable for laboratory tests of the scale undertaken in this project. The sampling frequency of the analyser was between 12.5 and 25 Hz for the tests.

Different techniques for laying the fibre optic cables were explored as two effects are known to influence the behaviour of the fibre. Firstly, the residual tension present in the fibre due to the laying technique and secondly, the coupling between the fibre and the surrounding soil. The base approach is to lay the fibres across the box and then to tape them to the box at each end of the layer (Figure 12).

The first technique attempted to improve this base approach, by coating the fibre in glue and then rolling it in sand, before laying the fibre into the box (Figure 13). This increases the friction angle of the fibre-soil interface and thereby improves the coupling with the surrounding sand.

The second technique involved removing the tape at the edges of the box in order to minimise the residual tension, leaving only residual tension due to the overburden pressure of the soil. This was further explored by allowing one fibre to leave the box via a tube, instead of passing through the body of the soil (Figure 14), thereby further minimising the residual tension by reducing the interface friction.

The final technique explored, was to introduce slack into the fibre in the vicinity of the trapdoor (Figure 15) thereby minimising the residual tension in the fibre, and improving the coupling by allowing easier movement of the fibre.

The results of this physical modelling study are discussed in Section 4.3.

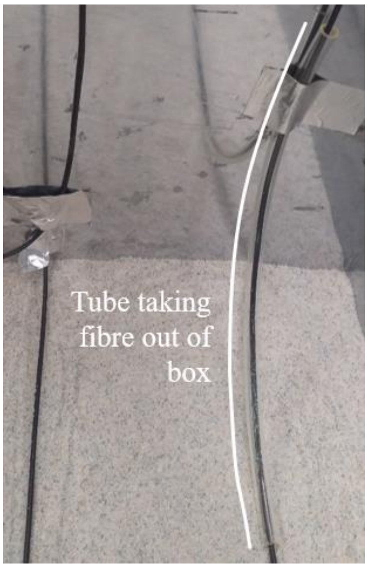

Figure 14: Fibre running via a tube out of the box.

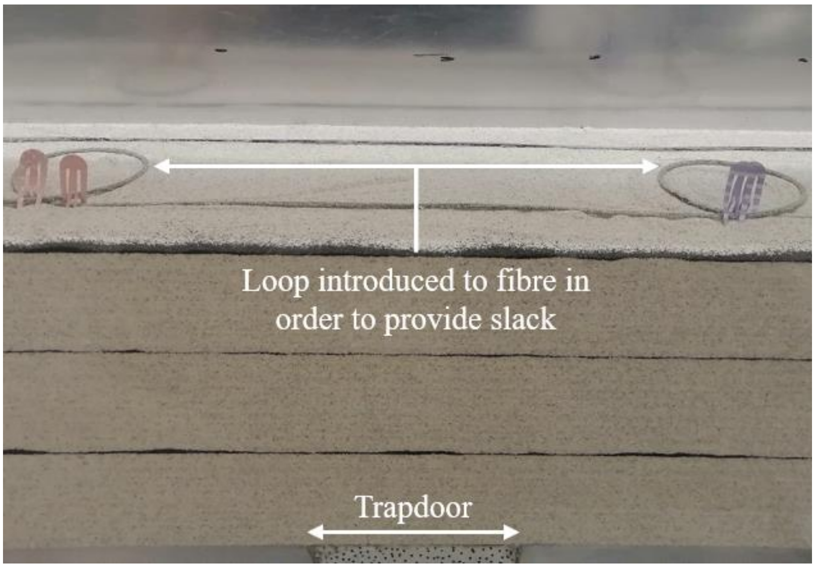

Figure 15: Fibre with slack introduced in the vicinity of the trapdoor.

Throughout the tests two fibres were laid in three layers for the plane strain trapdoor rig, as shown in Figure 16. For the TBM rig, two transverse fibres were laid in a similar pattern, but another two cables were laid in a longitudinal pattern as shown in Figure 17. The only exception to this layout was the second test where only one fibre was laid in three layers; the second fibre was only laid in the bottom layer. Throughout the tests the soil height was maintained as a constant relative to the trapdoor width and the tunnel diameter (see Figure 16 and Figure 17).

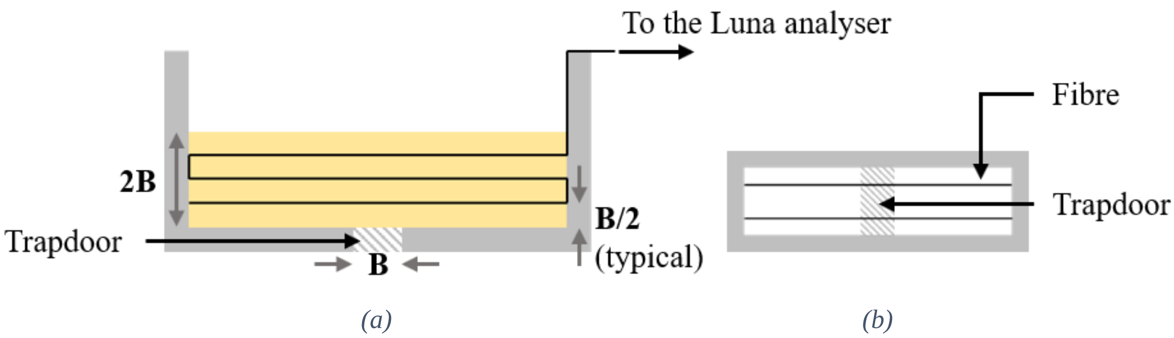

Figure 16: An elevation (a); and plan (b); view of the trapdoor fibre layout.

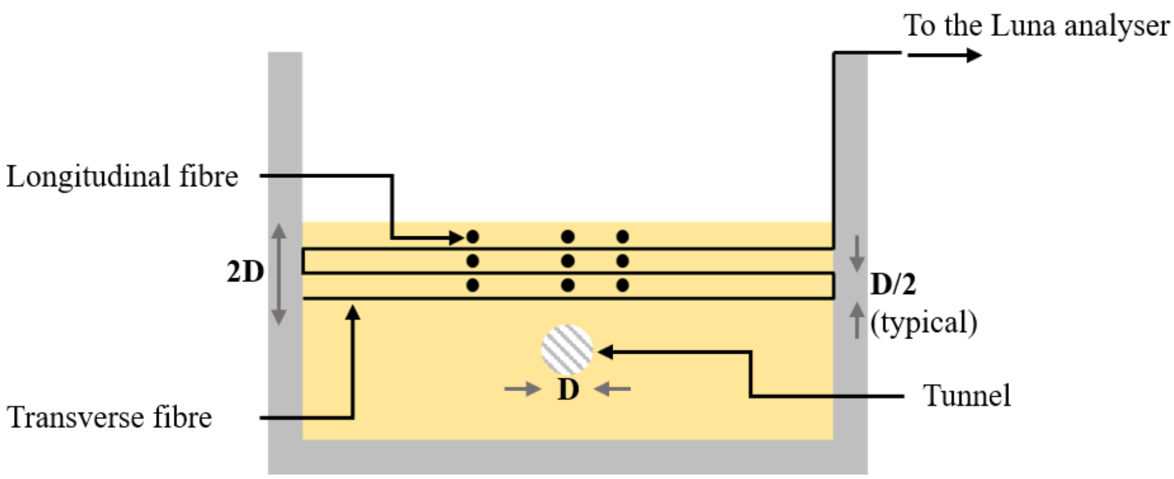

(a)

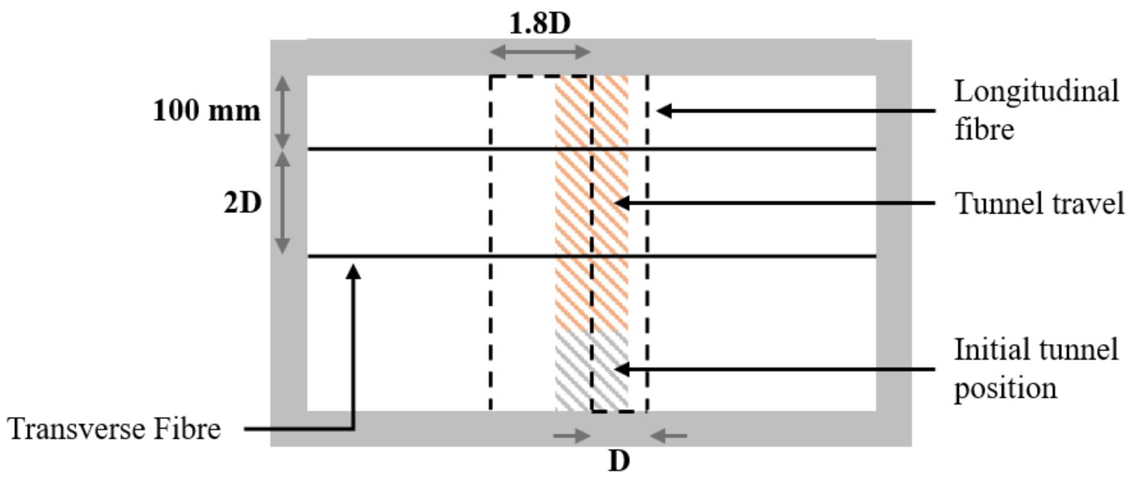

(b)

Figure 17: An elevation (a); and a plan (b); view of the tunnelling fibre layout.

3.2 Miniature TBM

A strong box with a miniature TBM was used to simulate the tunnelling process. The TBM incorporates a screw conveyor (Figure 18(a)) to transfer the excavated soil out of the box. The diameter of the tunnel is 76.2 mm. A motor is used to drive the TBM and an actuator pushes the tunnel into the soil. The tunnel is advanced at a constant speed enabling the position of the tunnel to be calculated at any given time. The box has internal dimensions of 780 x 460 x 620 mm (Figure 18(b)). An array of LVDTs can be used to measure the surface settlements. The sand extracted from the box is collected and used to calculate the volume loss. This rig is currently being developed in the Schofield Centre by Casey Shepheard and Ahmed Alagha.

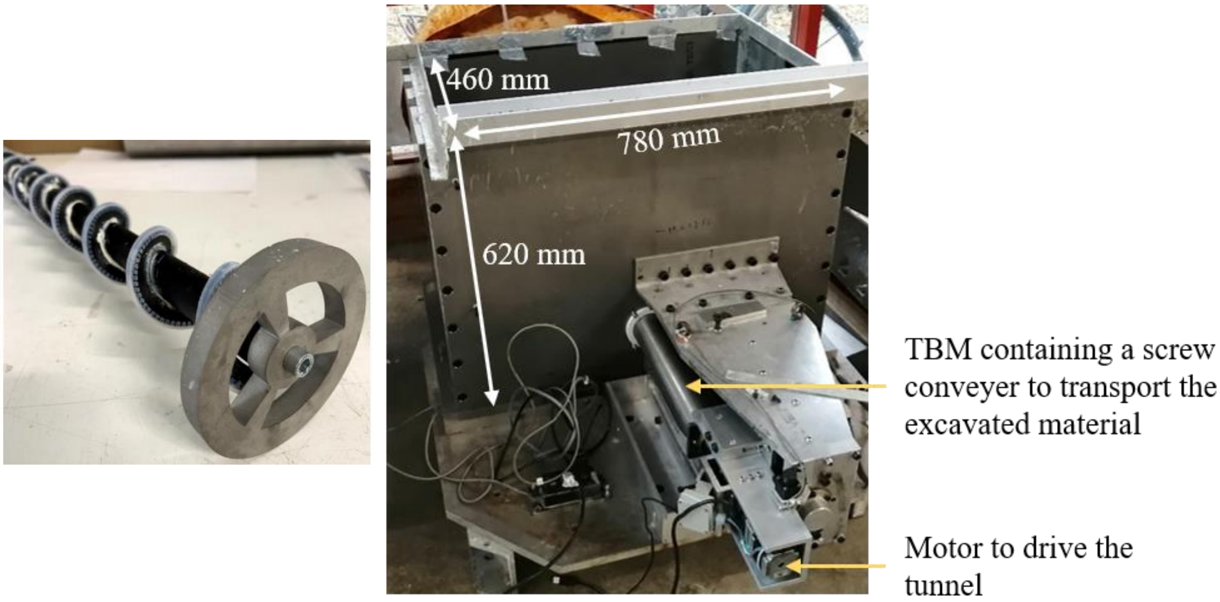

(a) *(b)*

Figure 18: The screw conveyer (a) (Ahmed Alagha); and the miniature TBM box (b).

3.3 Sample Properties

All the tests are performed using dry Hostun sand, which is fine-grained with the properties given in Table 3. The different test rigs were filled using the sand pourer (Madabhushi, Houghton and Haigh, 2006 and Zhao *et al.*, 2006) in order to obtain consistent relative densities. The only exception to this was Test 2, which was simply filled by hand in order to save time.

Table 3: Hostun sand properties (da Silva, 2017).

Property	**Symbol**	**Units**	**Value**
Coefficient of uniformity	C_u	-	1.43
Coefficient of curvature	C_c	-	1.03
Average particle size	d_{50}	mm	0.356
Minimum void ratio	e_{min}	-	0.555
Maximum void ratio	e_{max}	-	1.010
Specific gravity	G_s	-	2.65
Peak angle of friction	ϕ_p	o	48
Critical angle of friction	ϕ_c	o	35

When performing tests at 1g, the stress level in the soil does not scale properly to full-scale. For this reason, geotechnical experiments are usually performed in the centrifuge. However, when conducting tests at 1g, it is possible to compare the results to those at ng or full scale, using the following framework (Bolton, 1986):

$$I_R = D_R(10 - \ln p') - 1 \quad (11)$$

where I_R is the relative dilatancy, D_R is the relative density and p' is the mean stress level. In order for test results to be comparable the critical parameter is the relative dilatancy. This can be matched between the centrifuge and 1g by modifying the relative density, and hence means that tests at low relative density at 1g, correspond to a higher relative density in the field.

3.4 Test Programme

In total four tests were performed as outlined in Table 4. Each test uses different fibre laying and coating techniques as described in Section 3.1.2. A range of relative densities is used to explore the effect of this on sinkhole formation. However, Tests 3 and 4 were poured to similar relative densities to allow comparison of the sinkhole and tunnelling data. Unfortunately, the surface LVDT data for Test 4 was not obtained due to circumstances beyond the author's control and this has influenced the analysis performed (Section 4.5 and 4.6). The tunnel was also found to be under-excavating, leading to heave instead of settlement (Section 4.5).

Table 4: Testing programme.

Test	Rig	D_R (%)	I_R at trapdoor/tunnel level	Fibre Layout (see Section 3.1.2)
Test 1	Trapdoor	96	7.45	Two standard layout fibres; one coated with sand, and one uncoated
Test 2	Trapdoor	48	3.29	One standard layout fibre left untaped, and one single layer fibre leaving the box via a tube
Test 3	Trapdoor	52	3.64	Two standard layout fibres; both coated with sand and one with slack introduced in the vicinity of the trapdoor
Test 4	TBM	58	4.17	Two standard layout transverse fibres and two longitudinal layers all coated in sand

Table 5: Tests from published literature used for comparison and validation.

Author	Test No.	g-level	D_R (%)	I_R at trapdoor level
Della Ragione (2020)	gd3	1g	40	2.58
	gd4	1g	54	3.82
	gd5	1g	19	0.71
	gd6	1g	88	6.77
Da Silva (2017)	UNRNF-2	40g	87	4.08

The tests performed in this project are compared to relevant tests performed by Della Ragione (2020) and da Silva (2017) as outlined in Table 5. This enables both validation (Section 4.1 and 4.2) and further analysis of the effect of relative density (Section 4.6). Della Ragione's tests included fibre optic cables with the same layout as shown in Figure 16 using the base fibre laying approach (Figure 12). Both della Ragione and da Silva's tests used a PIV setup similar to the one shown in Figure 8(a).

4 Results and Discussion

4.1 Validation of new PIV technique

In order to validate the new PIV technique (Section 3.1.1) vertical settlements are plotted across the height of the box for two different trapdoor displacements. Test 3 (Table 4) was performed at a relative density of 52% enabling a comparison with gd4 (Table 5) which was performed at a relative density of 54% in otherwise identical sample conditions.

Figure 19 demonstrates that the new PIV data functions as expected, showing very good agreement both in shape and magnitude with the comparison test.

4.2 Validation of Testing Method

4.2.1 Repeatability

The repeatability of the experimental setup and the data collection techniques can be verified by comparison to the results of Della Ragione (2020). The settlements obtained as the sinkhole develops are very similar in both tests (Figure 19), lending confidence to the repeatability of the results.

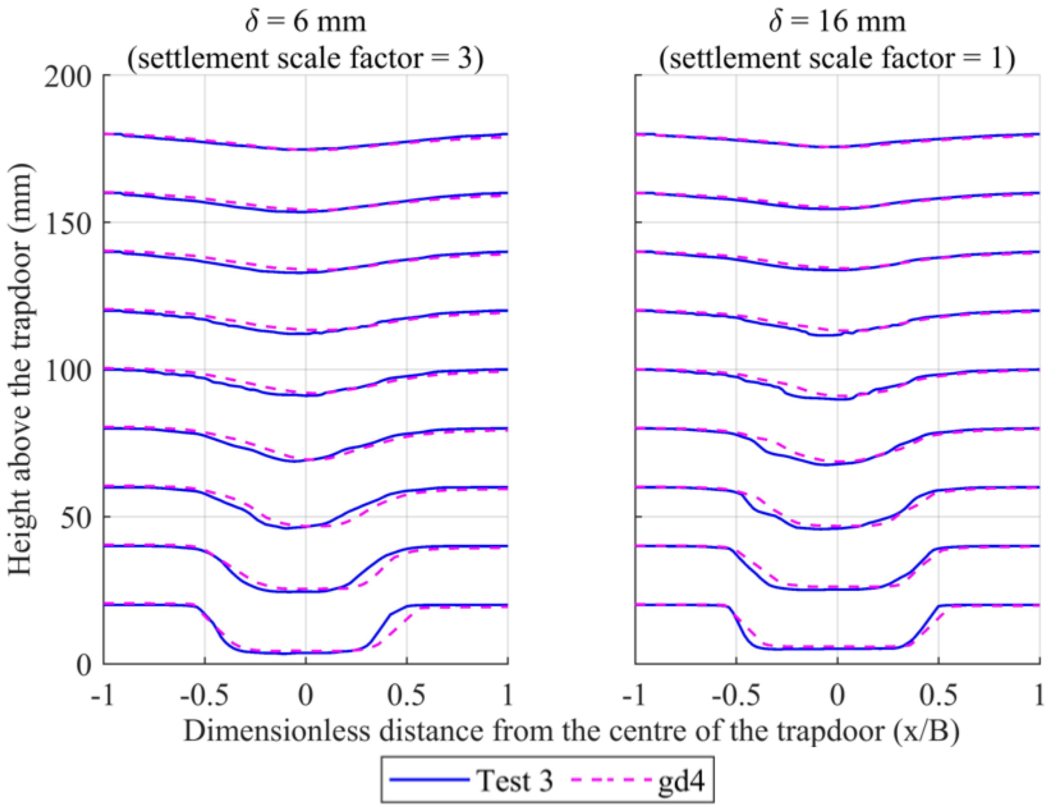

Figure 19: Settlements obtained from PIV data, for two trapdoor displacements, from Test 3 and gd4.

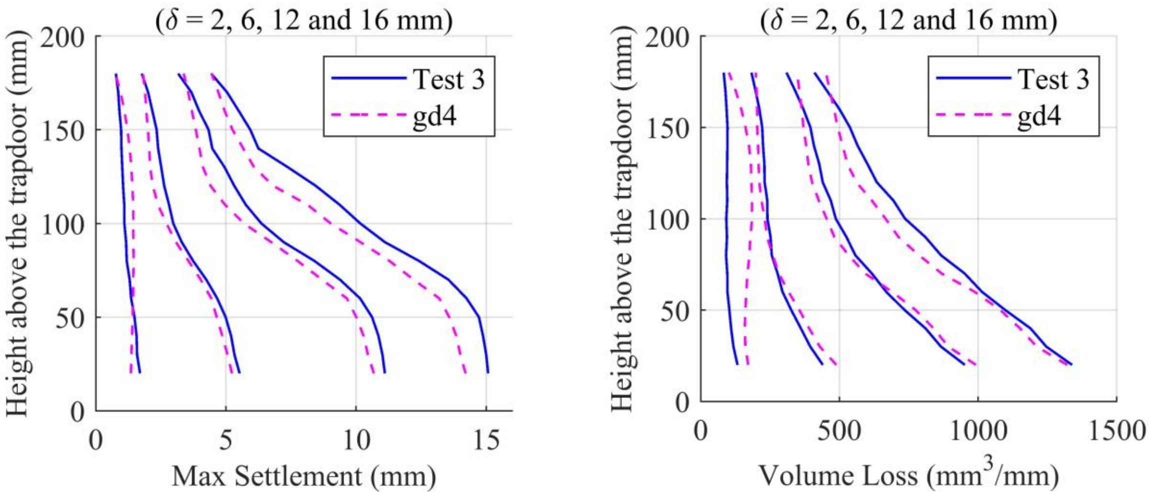

(a) *(b)*

Figure 20: Maximum settlements (a); and volume losses (b); obtained from PIV data, for different trapdoor displacements, from Test 3 and gd4.

The maximum measured settlements for different trapdoor displacements across the height of the box were extracted. Figure 20(a) compares the trend in maximum settlement for Test 3 with the results obtained by Della Ragione (2020). Both tests show similar trends and magnitudes with only slight discrepancies. These discrepancies are likely due to the difference in relative density between the two tests and differences in the PIV set-up.

The soil volume losses were obtained by calculating the area underneath the settlement profiles. Figure 20(b) shows a comparison of the volume losses with height, for different trapdoor displacements, between Test 3 and gd4. This indicates that the test is repeatable as the trends are similar across both tests. The volume loss comparison shows the greatest discrepancies between the two tests, particularly for low trapdoor displacements. It is known that the PIV data from gd4 was influenced by sunlight falling on the Perspex window (Della Ragione, 2019-2020) at the beginning of the test. This is the likely cause of the discrepancies.

4.2.2 Consistency

In order to demonstrate the consistency of the data with published literature, Test 3 is also compared with a test, performed at a higher stress level in the centrifuge, by da Silva 2017 (UNRNF-2) (Table 5). UNRNF-2 had the same soil height to trapdoor width ratio as Test 3, and hence is suitable as a comparison. In order to compare these tests, the relative dilatancies should be similar. It is possible to calculate the necessary relative density for the 1g test in order to achieve this using Equation 11. For the centrifuge test the relative dilatancy at the base of the model can be calculated as 4.1. This allows a suitable relative density for the 1g test to be

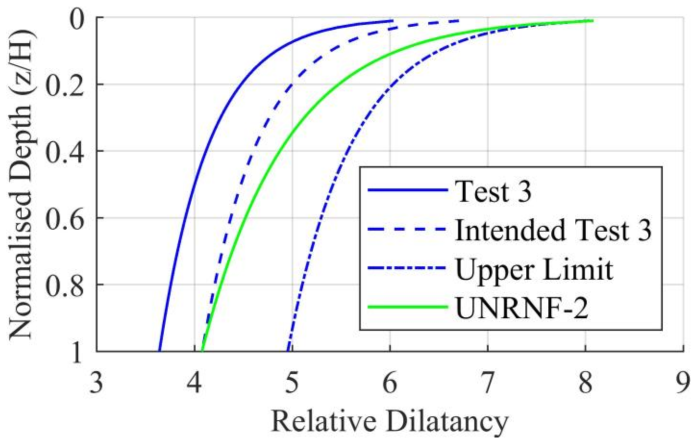

Figure 21: Relative dilatancy with height, for Test 3 and UNRNF-2.

calculated and gives 57%, which would lead to matching dilatancies at the base of the model (Figure 21). In this scenario the relative dilatancy of UNRNF-2 would be greater throughout the height of the model and hence this test would exhibit smaller settlements compared to Test 3. In order for the relative dilatancies to match at the surface a relative density of 67% is required (Figure 21). A relative density between 57% and 67% would thus lead to a match in relative dilatancy, between the two tests, somewhere along the height of the model.

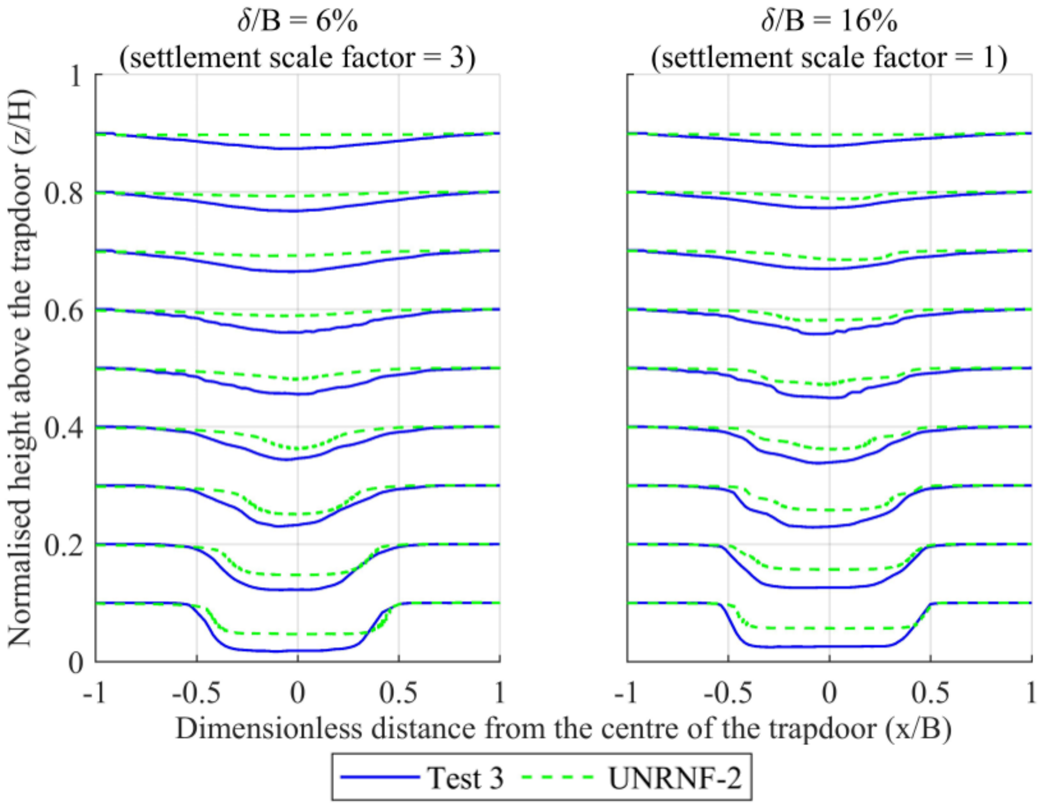

Figure 22: Settlements obtained from PIV data, for two trapdoor displacements, from Test 3 and UNRNF-2.

However, the relative density of Test 3 was 52% and hence leads to lower dilatancies throughout the height of the model (Figure 21). Thus, it is expected that UNRNF-2 exhibits lower magnitude settlements than Test 3. This is confirmed in Figure 22 which shows the comparison of settlements, obtained from PIV data. The difference in relative dilatancy is largest at the surface (Figure 21) and explains why UNRNF-2 shows very little surface settlements compared to Test 3 (Figure 22). The settlement trough shapes are consistent across the two tests, suggesting that the soil mechanisms at play are similar.

It is hence apparent that the behaviour of the sinkhole at 1g is exacerbated compared to the behaviour in the field and indicates that the 1g tests, when performed using this technique, provide conservative results.

4.3 Fibre Laying

To explore the effect of different fibre optic laying techniques on the strain profiles these have been plotted at the three heights at which the cable was laid and at three different trapdoor displacements early on in the test (Figure 23). The earlier stages of the test are of more interest as these are important for an early warning system.

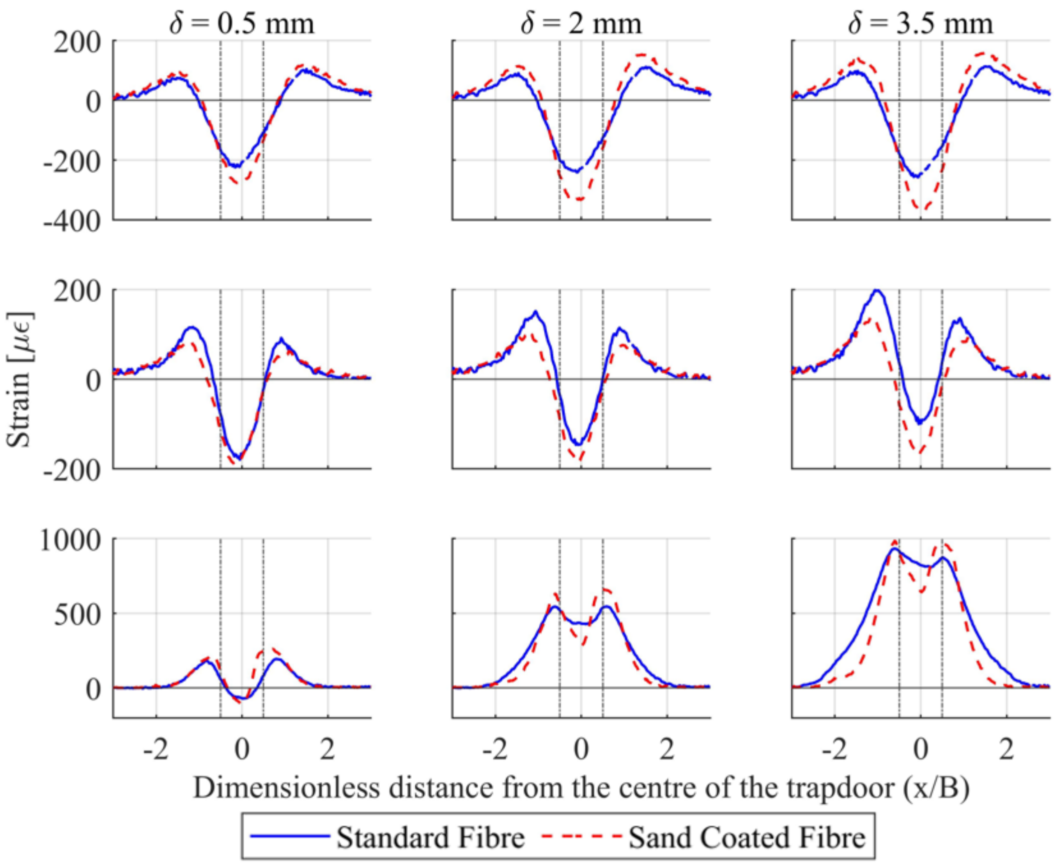

Figure 23: Fibre strains in the top, middle and bottom layer, for three different trapdoor displacements, in Test 1.

In the first test one fibre was laid as normal and the other was coated in sand before laying (Section 3.1.2). Both show a very similar response throughout the test; however, the sand coated fibre shows greater magnitude negative strains in both the top and the middle layer. The two peaks are also more apparent in the sand coated fibre, especially when looking at the bottom layer with a trapdoor displacement of 3.5 mm. These results indicate that coating the fibre in sand improves the interface friction between the fibre and the surrounding soil, allowing it to better capture the soil deformations.

In the second test, one fibre was left loose at the edges and the other left the box via a tube (Section 3.1.2). The results of this test are only plotted for the bottom layer as the tube fibre was only laid in one layer (Figure 24). The loose fibre shows greater magnitude negative strains when looking at a trapdoor displacement of 0.5 mm. However, the tube fibre shows greater magnitude positive strains later on in the test. Both of the fibres show a similarly pronounced double peak.

A comparison between the two tests (Figure 23 and Figure 24) indicates that the strain profiles are wider in the second test. This is consistent with the lower relative density of the second test (48% compared to 96%), as this reduces the overburden pressure and hence reduces the interface friction between the fibre and the soil. It is also worth noting that in both tests the fibre strain profile reaches, or is close to, zero before hitting the edge of the box. This suggests that the overburden of the soil provides sufficient resistance to movement of the fibre, in order to limit the zone of influence to the confines of the box. Therefore, it is observed that the fixing

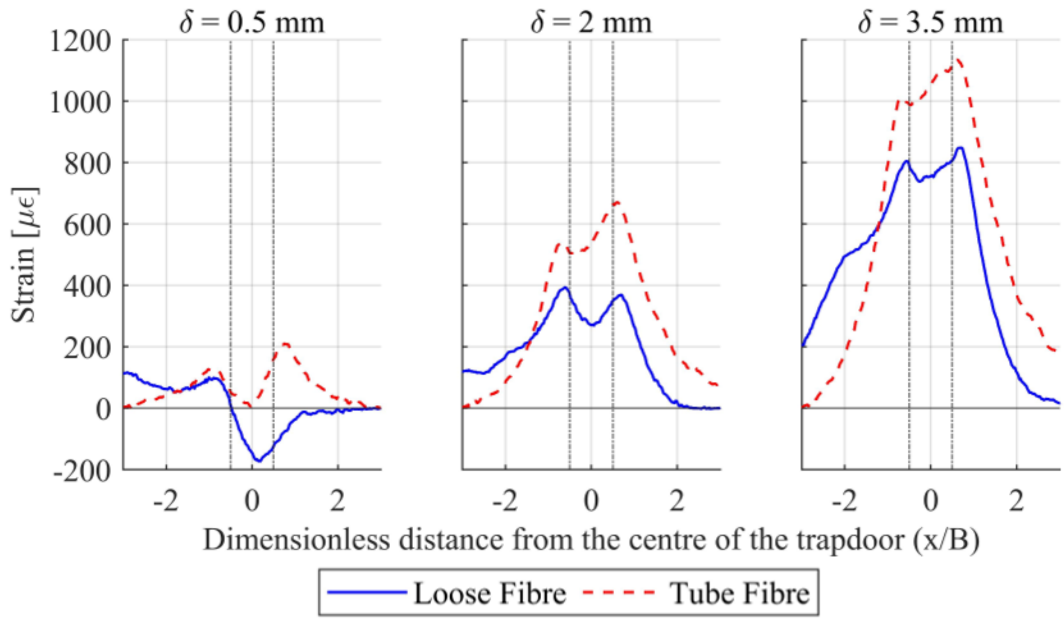

Figure 24: Fibre strains in the bottom layer, for three different trapdoor displacements, in Test 2.

method does not have a large impact on the results. The important factor is in fact how taut the fibres are laid. It was thus concluded that it is preferable to minimise the pretension of the fibres; however, it is desired that the fibres lie in a straight line and a certain amount of pretension is required to achieve this. This is easier to achieve with the fibres taped at the edges.

In the third test both fibres were coated in sand and taped to the edges of the box, based on the results from the first two tests. However, one of the two fibres had slack introduced in the vicinity of the trapdoor with the intention of improving the coupling between the fibre and the surrounding soil (Section 3.1.2). The results of Test 3 are presented in Figure 25. Both fibre strain profiles exhibited a similar response. The loose fibre has a slightly larger negative response early on, but the most obvious result is that the loose fibre remains centred around the zero-strain mark for longer (see the bottom and middle layers at a trapdoor displacement of 2 mm). This suggests that the slack introduced in the vicinity of the trapdoor does indeed

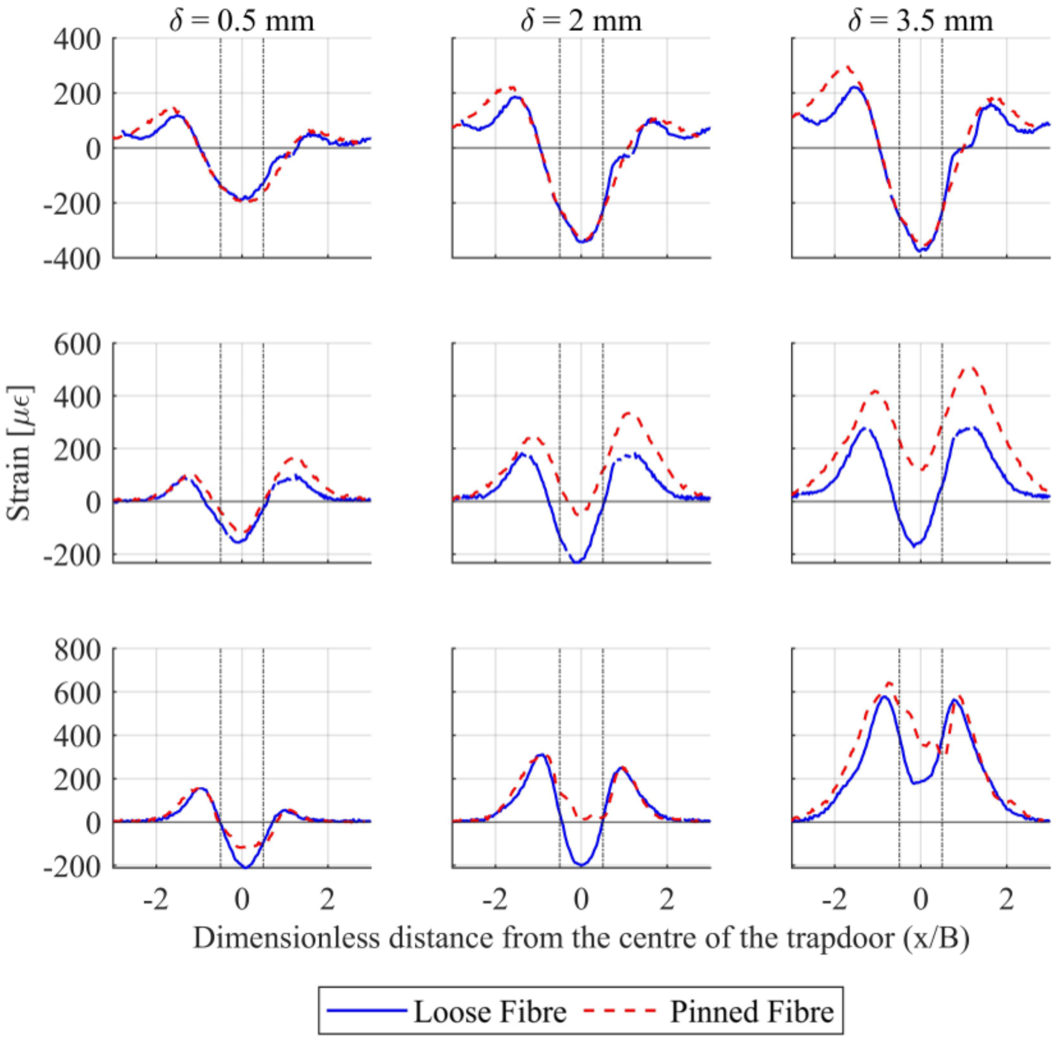

Figure 25: Fibre strains in the top, middle and bottom layer, for three different trapdoor displacements, in Test 3.

improve the coupling of the fibre, as it takes longer for this fibre to experience the increase in tension that shifts the profile upwards. However, the disadvantage of introducing slack is that it is harder to interpret the resulting data, as the fibre is no longer in a straight line and hence points on the fibre are harder to correlate with locations in the box.

Summary

Different techniques for laying fibres were explored and analysis of the results led to the following conclusions:

- Increasing the interface roughness of the fibre is beneficial as this improves the coupling with the soil.
- The fibre strain profile fits within the confines of the box, demonstrating that the fixing method does not disrupt the data as long as the tautness of the fibre is kept to a minimum.
- Introducing slack into the fibre improves the ability of the fibre to follow the soil deformations; however, it increases the difficulty of mapping points on the fibre to locations in the box.

Further Research

In order to further explore different techniques for fibre optic laying, introducing slack into the cable whilst maintaining ease of point mapping could be explored in the laboratory. This research should be combined with field testing of the proposed techniques.

4.4 Sinkholes

4.4.1 Settlement Behaviour

As discussed in section 2.2.4 it is possible to apply the gaussian fit to the settlements obtained during sinkhole formation. Figure 26(a) compares the raw PIV data with a standard gaussian fit (Figure 6) and a modified gaussian fit (Equation 6). It is visible that for the bottom layer the modified gaussian provides the best fit. This is confirmed in Figure 26(b), showing that the modified gaussian is a considerably better fit for the bottom layer, in particular as the trapdoor displacement increases; whereas both fits work equally for the other layers. This aligns with the results found in literature, suggesting that the steeper settlements experienced in sand can be better fitted using a modified gaussian. As the distance above the trapdoor increases the settlements experienced become less steep and hence, they can be equally well fitted by the standard gaussian. For the purpose of this report the modified gaussian has been used.

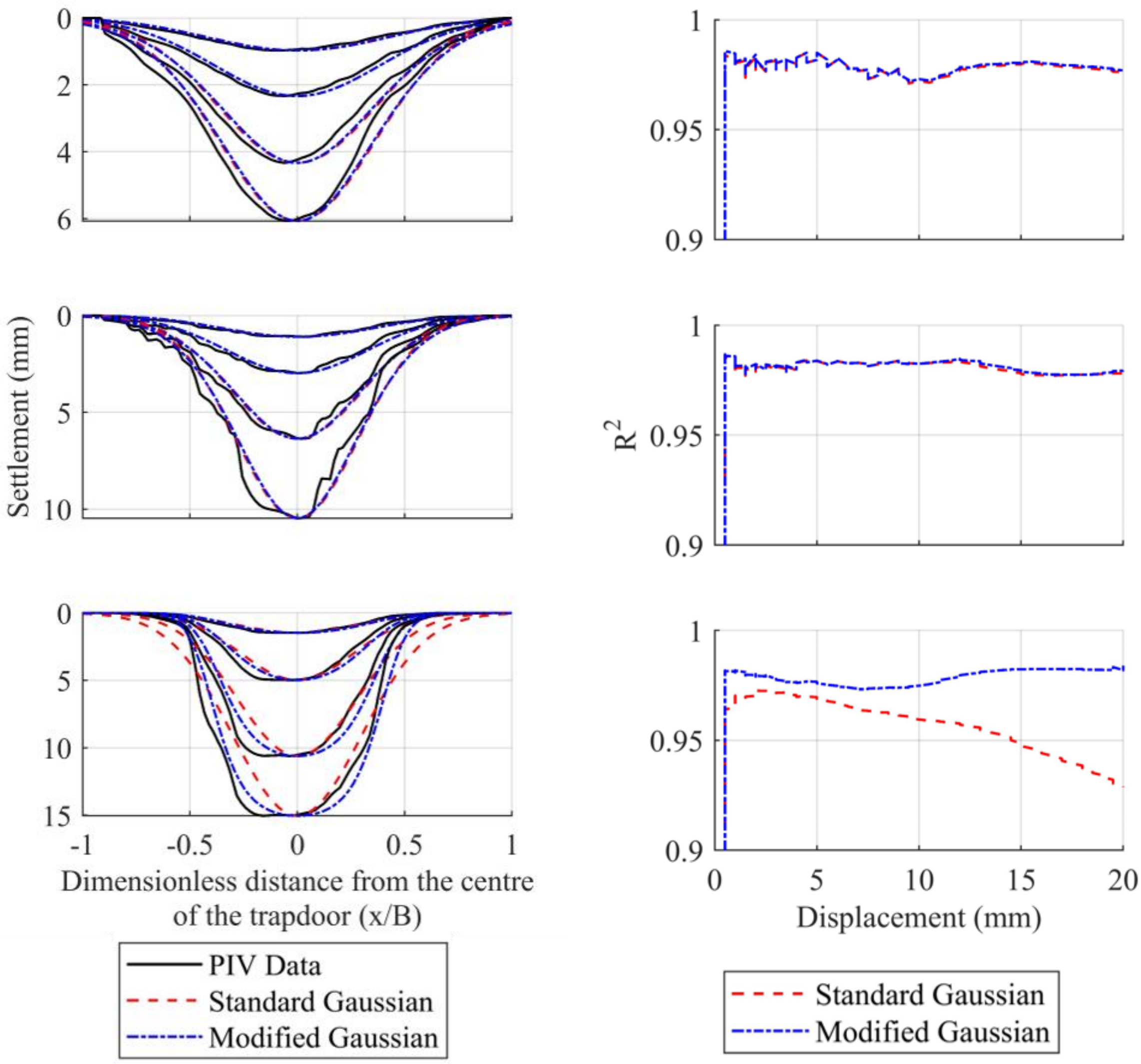

(a) *(b)*

Figure 26: The raw settlement data, the standard gaussian fit and the modified gaussian fit for trapdoor displacements of 2, 6, 12 and 16 mm (a); and R^2 values for the two gaussian fits (b); at the top, middle and bottom layer for Test 3.

During the formation of a sinkhole the ground also experiences horizontal displacements, and these can similarly be characterised using a gaussian equation. The following equation, from Klar, Dromy and Linker (2014), was used:

$$S_h = k \frac{x}{z} S_v \qquad (12)$$

where S_h is the horizontal displacement, k is a factor and z is the height above the trapdoor. Figure 27 compares the raw PIV data, and the gaussian fit for the horizontal displacements, indicating that this equation provides a good fit to the observed results.

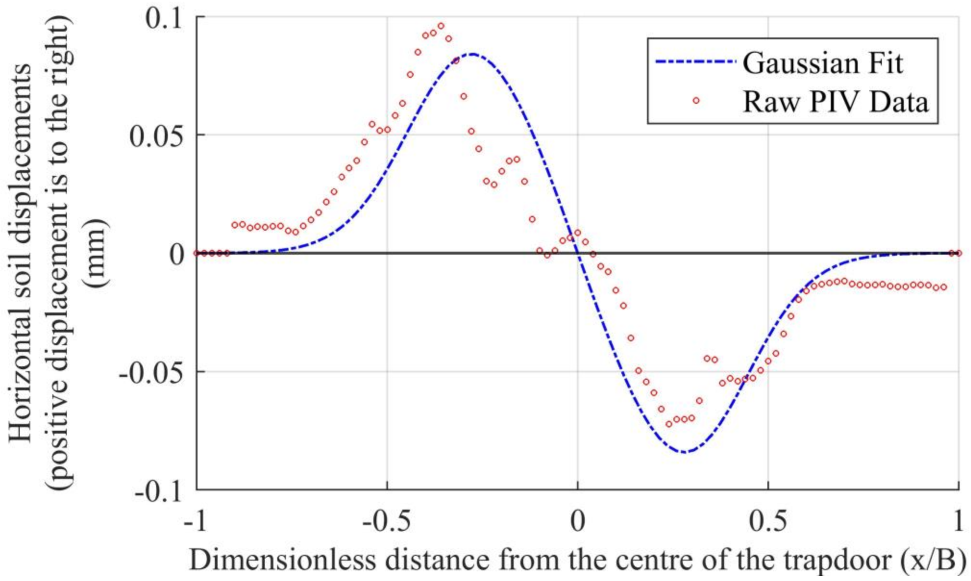

Figure 27: The PIV horizontal displacements and the gaussian fit using Equation 12 for Test 3.

4.4.2 Strain Profile

The strain profiles from the fibre optic cables have a consistent shape across tests and heights. See the top left plot in Figure 28 for the strain profile development throughout Test 3. All of the strain profiles are characterised by a double peak. Initially the profile is negative in the region of the trapdoor and eventually the fibre experiences more and more tension leading to the strain profile moving out of the negative zone.

To explore the significance of the fibre strain profiles, the PIV settlement data has been converted into strain profiles, using the gaussian fits in order to minimise noise. They have been converted into vertical, horizontal, and combined strains in order to explore how the fibre behaves. The fibre has a very low stiffness perpendicularly and hence can follow vertical movements. This is particularly important for this application, where most of the ground movement is expected to be vertical. However, the fibre has an axial stiffness of 200 MPa and hence horizontal movements along the length of the fibre generate strains as the fibre is stretched.

The righthand plots in Figure 28 compare the vertical and horizontal strain profiles obtained from the PIV data. It is apparent that the two profiles are very different. Although both have a double peak the vertical peaks are within the trapdoor extents whereas the horizontal peaks are outside of the trapdoor extents. More importantly, the vertical strain profile does not exhibit any negative strains whereas the horizontal profile does. Finally, it is also worth noting that the magnitudes of the horizontal strains are considerably larger than the vertical strains. This

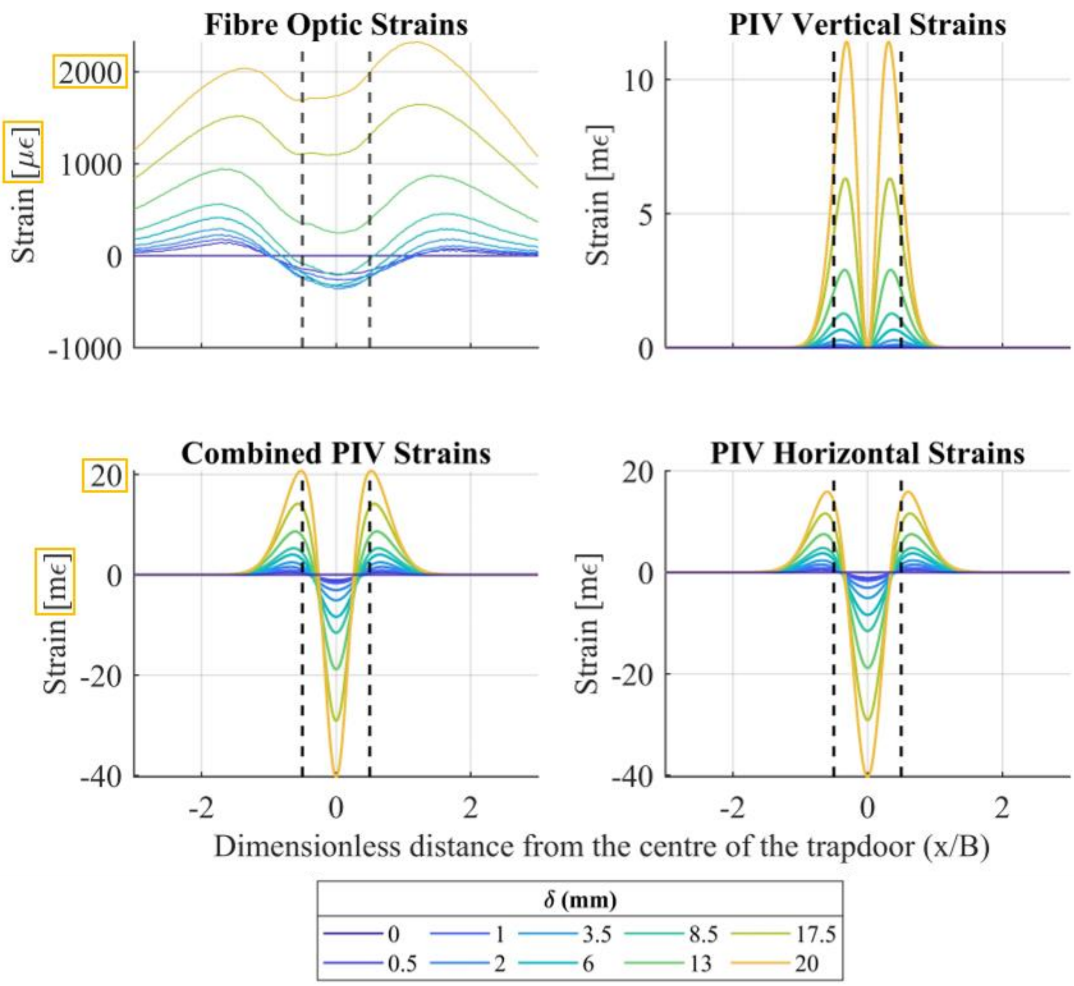

Figure 28: Fibre strain profile for the rear fibre (top left); vertical (top right); horizontal (bottom right); and combined (bottom left); strain profiles obtained from the PIV data, all for the top layer, in Test 3.

suggests that the horizontal strains are dominant, and this is confirmed by the fact that the combined strain profile (bottom left in Figure 28) is very similar to the horizontal profile. Furthermore, the fibre strain profile contains negative regions which are only present in the horizontal profile. Accordingly, it appears that the fibre optic cable is measuring the horizontal strains.

However, when comparing the horizontal PIV strain profile with the fibre strain profile in Figure 28, there are several important differences. Firstly, the PIV strains are approximately one order of magnitude larger than the fibre strains. Secondly, the fibre strain profile appears to be significantly wider than the PIV profile, with the peaks occurring at 1.5 compared to 0.6. Finally, it is also noticeable that the fibre behaviour is different to the PIV behaviour, as the strain profile does not stay centred on the zero-strain axis as it does for the PIV. This proves that the DFOS data cannot be used directly for sinkhole detection, and that further processing is required.

There are several conclusions which can be drawn from this data. It is apparent that there is slipping along the fibre-soil interface which leads to the difference in strain magnitudes. The soil is able to displace far more than the fibre and hence can experience far higher strains. The results also suggest that the fibre-soil interaction leads to a change in the settlement of the soil, indicating that the settlements 'seen' by the PIV at the edge of the box are different to those experienced by the soil around the fibre. This would account for the difference in profile widths. Finally, the fact that the fibre profile does not stay centred on the zero-strain axis suggests that as the soil displacement increases, this leads to the fibre pulling in from the edges of the box causing tension along the length of the fibre and hence leading to a 'rise' in the fibre profile.

4.4.3 Viability of an early warning system

It is apparent from the previous sections that the fibre optic data obtained during the plane strain trapdoor tests contains a signature strain profile which is easily identifiable in laboratory testing. Field testing is required in order to verify whether this signature can be easily identified in the field, over greater length scales and with other ground disturbances occurring. If this signature is easily identifiable in the field, then using DFOS to identify sinkholes becomes a viable strategy, as it is possible to locate the centre of the sinkhole using the fibre data.

However, determining the size and depth of the sinkhole from the fibre optic data is more complicated. As noted in Section 4.4.2, the fibre strain profile is significantly wider than the PIV strain profile, making it hard to identify the depth and size of the sinkhole from the fibre data alone. This was further explored by tracking the location of the strain peaks obtained from the horizontal PIV strain data and the fibre data (Figure 29). The strain peaks from the PIV data show a consistent trend with height and trapdoor displacement, with the location centred around the trapdoor width. The fibre data strain peaks show a similar trend but sit considerably further outside the extents of the trapdoor. Although the fibre and the PIV data are not directly related, and hence a relationship between these trends has not been found, it is clear that the fibre optic data is conservative, indicating a wider sinkhole than is actually the case. This is beneficial for an early warning system as it demonstrates that the fibre data provides a conservative solution for detecting and predicting the size of the affected area. It is hence proposed to use DFOS to locate sinkholes and then to use a different technique such as GPR to accurately determine the size and depth of the sinkhole.

The closer the fibre is to the level of the trapdoor the more accurate the width prediction becomes. Figure 29 shows that, for low trapdoor displacements, the peak strain locations are

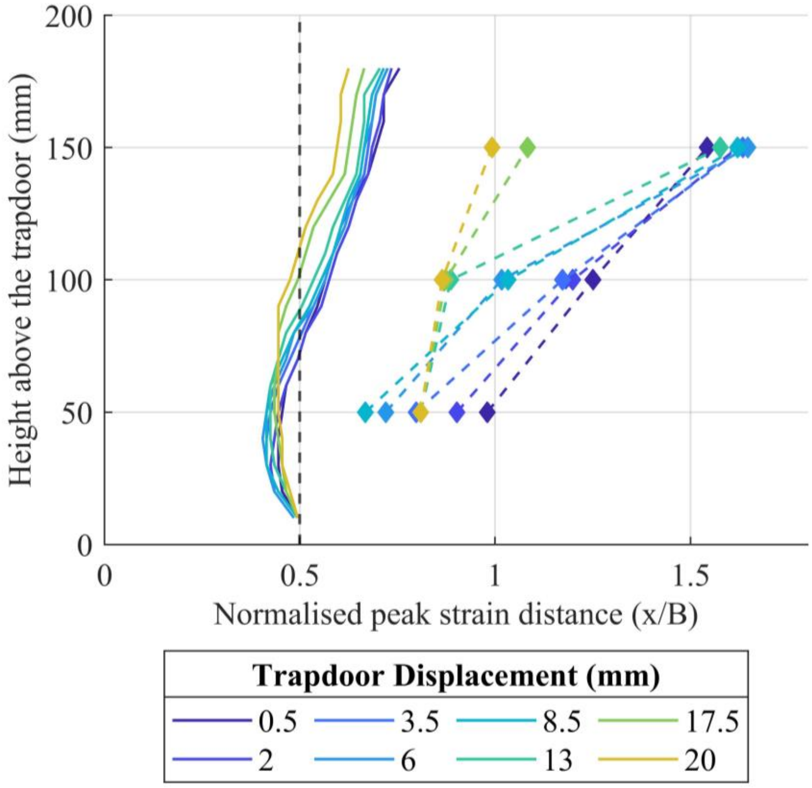

Figure 29: Strain peak locations with height for Test 3, comparing the PIV data (solid lines) to the fibre data (dashed lines).

directed towards the trapdoor width at the level of the trapdoor, indicating a potential trend which could be used to identify the depth and width of the trapdoor. Further tests with fibres laid at different heights, and with varying trapdoor widths, are necessary to verify this result.

Whilst exploring the behaviour of the fibre and PIV data, an interesting trend was outlined. It is possible to obtain the maximum gradient of the gaussian fits to the PIV settlement data, and then to locate the points which have 50% of this maximum gradient. It was discovered that these 50% maximum gradient points sit on, or close to, the width of the trapdoor throughout all

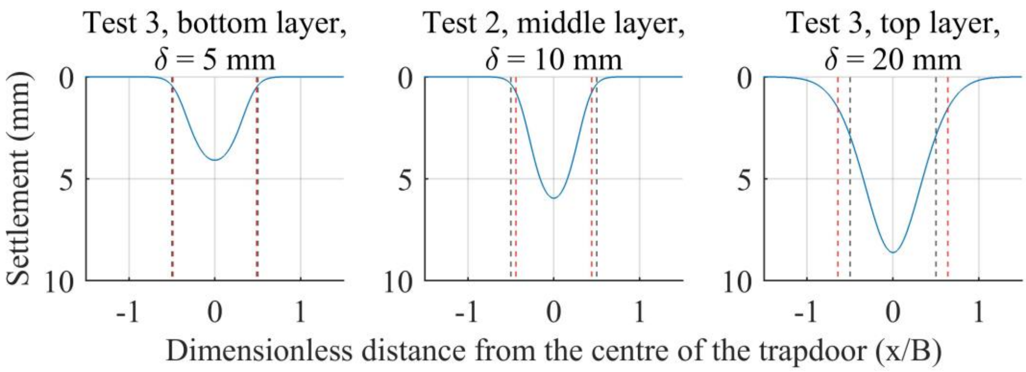

Figure 30: Gaussian fits (solid blue line) with the 50% max gradient location indicated (red dashed lines) in relation to the trapdoor (black dashed lines).

tests and all trapdoor displacements (Figure 30). To date, the author has not been able to find a distinct link between the trapdoor extents and these points.

Summary

The geomechanics of sinkhole formation have been explored using PIV and fibre optic cables. The following conclusions can be drawn:

- 1g testing can successfully simulate the sinkhole formation process enabling quick, easy data to be obtained.
- 1g testing facilitates the use of fibre optic cables as it avoids the complexities associated with installing fibre optic cables in the centrifuge.
- The modified gaussian fits the PIV settlement data well throughout the test and at all soil depths.
- It is possible to use a horizontal gaussian fit for the horizontal soil movements.
- The fibre optic data contains a signature strain profile which is easily identifiable in the laboratory.
- The fibre optic data is comparable with the horizontal strains calculated from the PIV data.
- The centre of a sinkhole can be accurately located using DFOS and this can be combined with another detection method such as GPR to size the sinkhole.
- The width of the fibre optic strain profile is larger than the width of the sinkhole providing a factor of safety.
- The soil in the vicinity of the fibre optic cable behaves differently to the soil at the edge of the box 'seen' by the PIV.

Further Research

The next step of this research consists in determining whether the signature strain profile is easily identifiable in the field, by performing field tests using a fibre layout informed by Section 4.3. The relationships between the fibres and the PIV should also be further explored to clarify whether there are direct links between the two, thereby enabling a sinkhole to be accurately located and defined by the fibre optic cables. Both of these steps are required to further confirm that DFOS would work as an early warning system for sinkholes. Further research could also be conducted on an improved rig using a raspberry pi camera setup to enable collection of detailed surface settlement data. Furthermore, a pressure bag could be incorporated to allow 1g tests to be performed at higher stress states.

4.5 Tunnelling

Further exploration of the fibre optic data was enabled by running a tunnelling test. In this test (Test 4) the TBM was under-excavating – extracting too little soil and thus pushing the soil out of the way instead of extracting it – hence, instead of the typical settlement profile as would be expected in tunnelling, heave was experienced. This does not occur in the field, apart from in exceptional circumstances, but can occur in the laboratory. In the case of heave, once the tunnel has passed underneath the soil begins to settle again. The magnitude of this post-heave settlement can vary. However, despite this being unlikely to occur in the field, the data from the test still demonstrates what the DFOS data is capable of. Due to issues with logging of the LVDT data during this test, it was not possible to determine exactly how much the soil heaved and then settled and due to the closure of the Schofield Centre following the Covid-19 outbreak, it was not possible to retake the test (see Appendix 2). Nevertheless, selected analysis of the collected data was performed and is presented below, as this still informs on expected strain profiles from the DFOS.

4.5.1 Transverse Strain Profile

The transverse fibre strain profiles obtained in the tunnelling test can be split into two phases. The first phase is during the approach of the tunnel. Figure 31 plots the strain development within the fibre as the tunnel approaches. The soil is heaving during this phase and hence it is expected that the fibre will be put into tension as it is dragged upwards with the surrounding soil. This is confirmed in Figure 31 where the strain above the tunnel increases in magnitude as the tunnel approaches. The shape of the profile is assumed to be dominated by the horizontal movement of the soil which explains the two troughs on either side of this peak. These are likely caused by the soil moving outwards, away from the heave, thus slackening the fibre at the edges. This is further confirmed when comparing Figure 31 with the fibre profile in Figure 28, as the strain profiles are effectively ‘flipped’, with two peaks becoming two troughs and one trough becoming one peak.

The second phase is once the tunnel has passed beneath and is travelling beyond the fibre (Figure 32). The behaviour of the ground changes substantially during this phase. The fibre strain profile starts from the same position that it ended in Figure 31 after having experienced

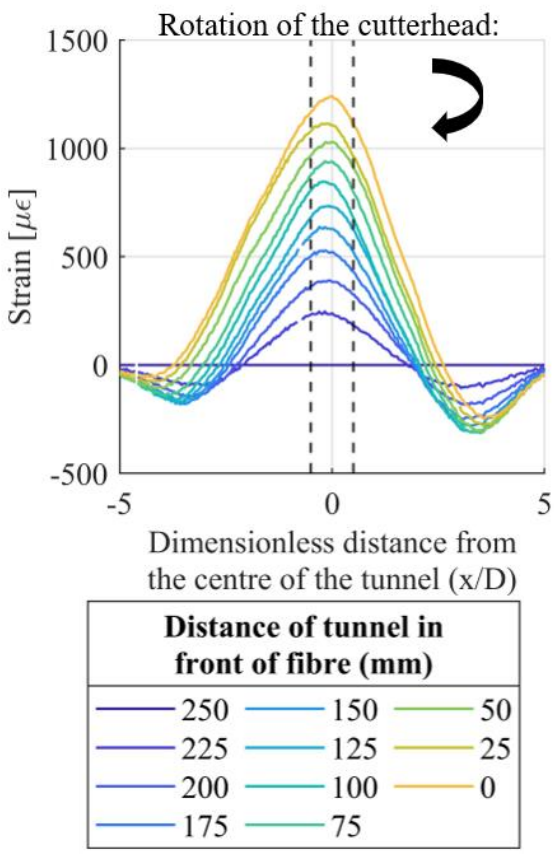

Figure 31: Strains measured by the fibre optic cable, in the top layer, rear cable, as the tunnel approached the cable.

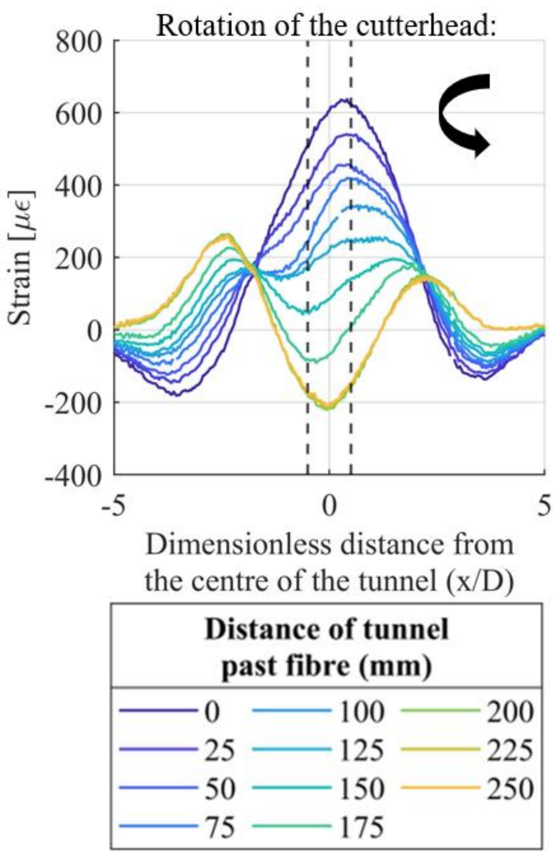

Figure 32: Strains measured by the fibre optic cable, in the middle layer, front cable, as the tunnel travelled beyond the cable.

heave. However, instead of the peak growing further and eventually levelling off it starts to reduce in magnitude, suggesting that the heave is shrinking. Gradually, two new peaks form leaving a trough between them, at which point the strain profile is readily comparable with the fibre profile in Figure 28. This suggests that the soil is beginning to take on a settlement profile. It is interesting to note that the location of the two peaks does not match with the locations of the initial troughs, indicating that the final settlement trough is narrower than the initial heave.

Another important factor influencing the fibre strain profiles is the rotation of the cutterhead, as this impacts the soil displacements. Figure 33 shows three sets of strain profiles from Test 4 with the rotation of the cutterhead marked on it. It is clear that the rotation of the cutterhead shifts the strain peaks. When the cutterhead rotates clockwise the peaks are shifted left and when it is rotating anticlockwise the peaks are shifted right. This result was consistent throughout the data proving that the direction of rotation of the cutterhead can be identified from the fibre data.

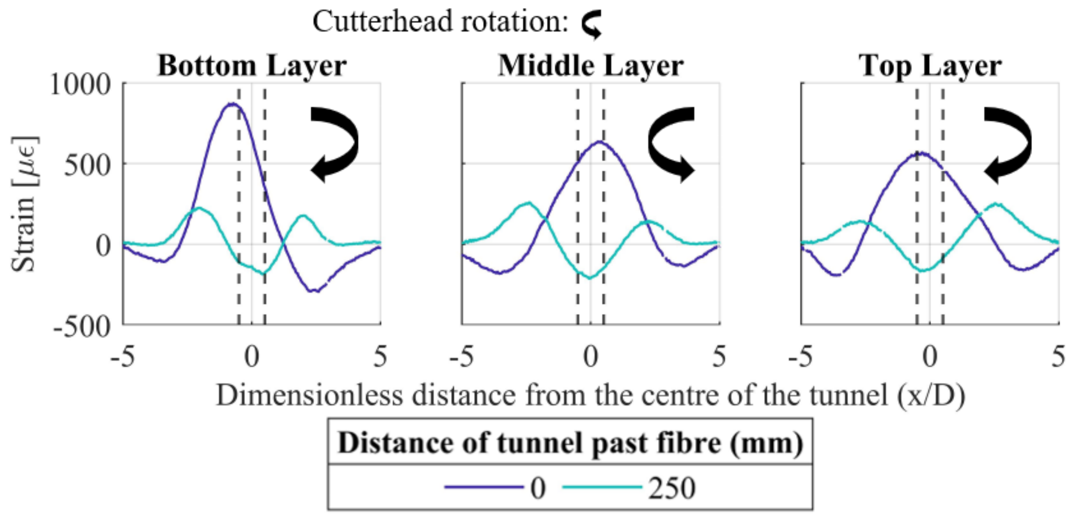

Figure 33: Strains measured by the front fibre optic cable.

4.5.2 Longitudinal Strain Profile

In order to analyse the longitudinal fibre strain data, obtained in Test 4, understanding of the longitudinal soil displacement profile is needed. As the LVDT data from this test is not available, it is necessary to use similar data obtained in a different test. Casey Shepheard (a PhD student in the Schofield Centre) has performed other tests on the same rig, and one of those also led to heave instead of the usual settlements. Figure 34 shows the longitudinal heave profile obtained using the LVDTs in that test. However, in order to calculate strains and compare to the fibre optic data it is also necessary to obtain a profile for the horizontal soil movements. In tunnelling literature, the longitudinal settlement profile is approximated using Equation 4 and the horizontal displacement profile is given by the following equation (Klar, Dromy and Linker, 2014):

$$S_l = n\frac{i_y S_{max}}{\sqrt{2\pi z}} exp\left(-\frac{1}{2}\frac{y^2}{i_y^2}\right) \tag{13}$$

where S_l is the horizontal soil displacement and n is a factor relating horizontal to vertical displacements. In order to determine the necessary variables for Equation 13, Equation 4 was used to create one standard settlement profile, and one inverted settlement profile – to simulate heave – which, when combined can be used to fit the LVDT data (Figure 34). Using the variables for the two settlement profiles, two horizontal displacement profiles were used to estimate the shape of the horizontal displacements (Figure 34).

It is then possible to convert the settlement profiles into a vertical and a horizontal strain profile (Figure 35). As observed in Section 4.4.2 it is notable that only the horizontal strain profile

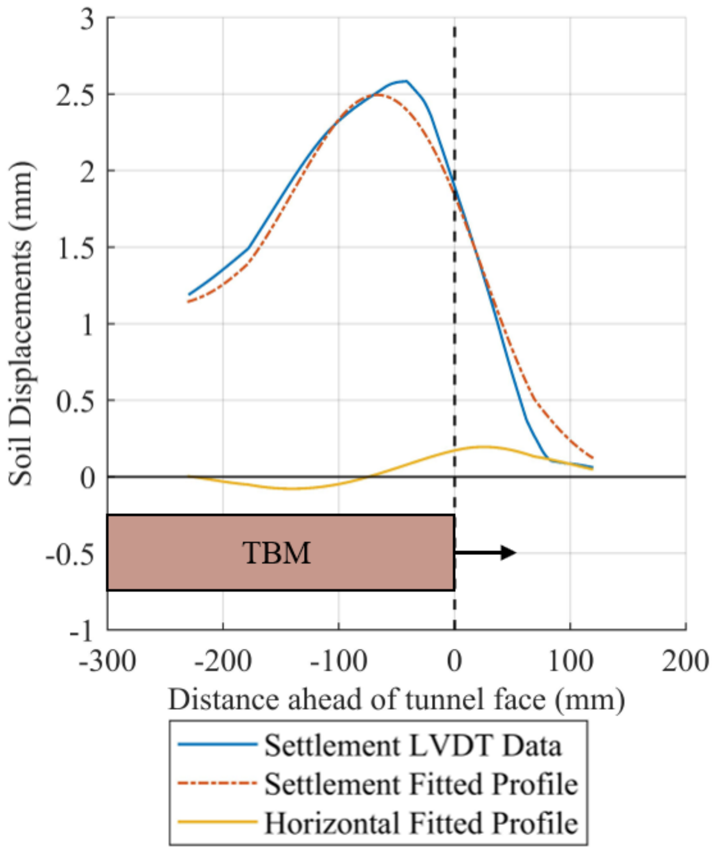

Figure 34: Vertical and horizontal soil displacement profiles obtained using LVDT data, from a separate test, performed by Casey Shepheard, on the same rig.

shows negative strains and once again the horizontal strain profile is several orders of magnitude larger.

Figure 36 shows the fibre optic longitudinal strain profiles obtained in Test 4 as the tunnel advances. See Section 3.1.2 for an outline of the fibre layout in Test 4. Once again, there is a

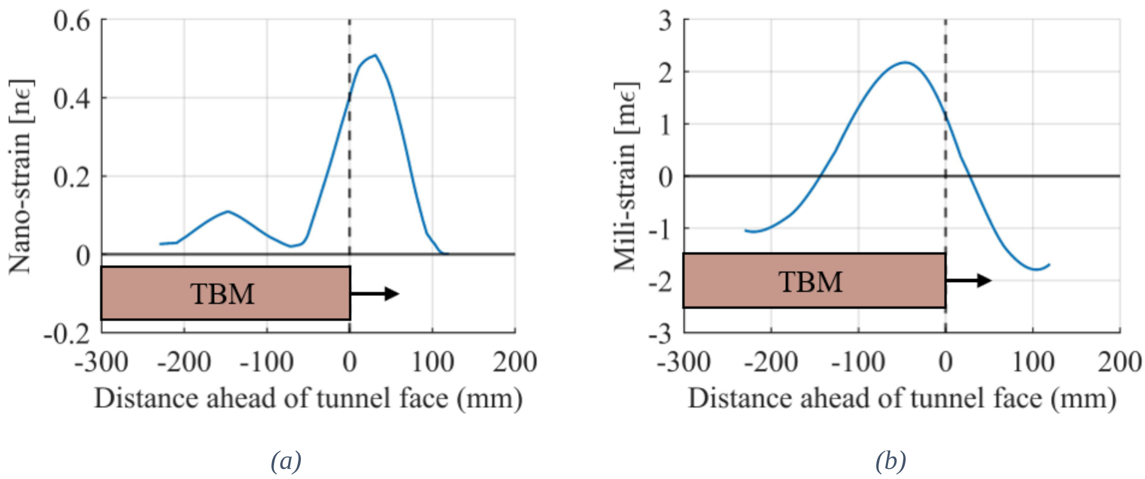

Figure 35: Vertical strain profile (a); and horizontal strain profile (b); derived using LVDT data.

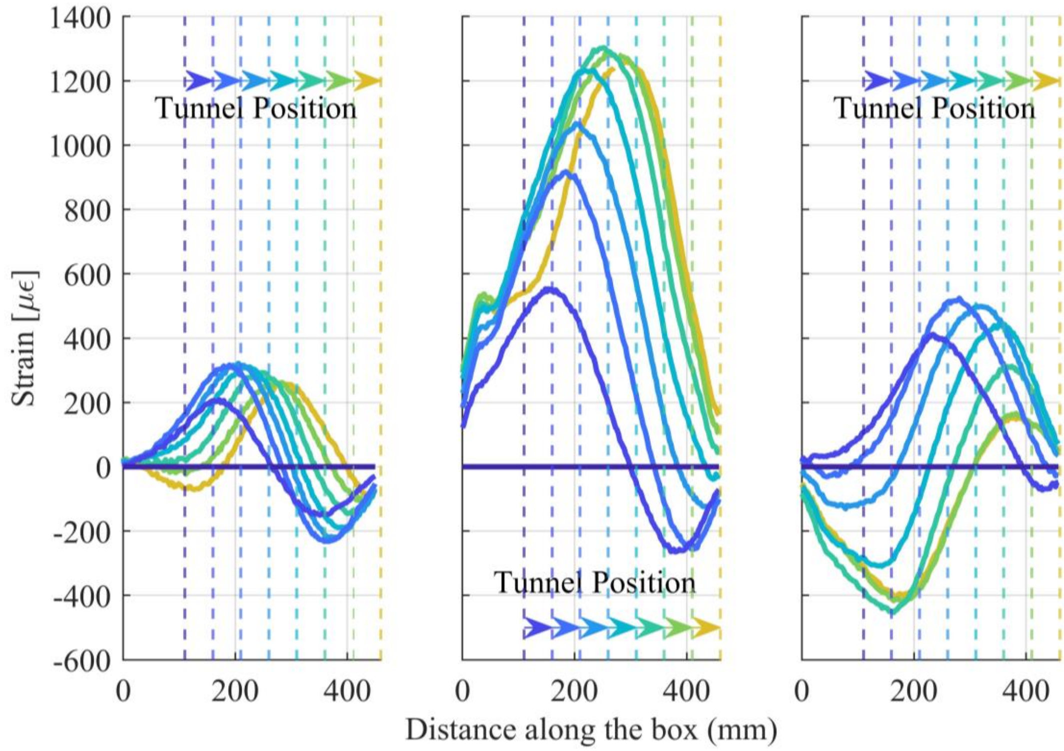

Figure 36:Fibre strain profiles, obtained for test 4, as the tunnel advances, for the bottom layer outer cable (left); the middle layer middle cable (middle); and the top layer inner cable (right).

consistent shape across the different locations of the fibres. Upon comparison of Figure 36 with Figure 35(b) it is again clear that the fibre strain profile shows many similarities with the horizontal strain profile. They both exhibit negative strains and contain one distinct peak instead of two. The fibre profile also appears to contain troughs either side of the main peak, although these reach the edges of the box and are hence less well defined. It is worth noting that, as expected, the fibre strain magnitudes are considerably lower than those obtained from the LVDT data.

Summary

The results from Test 4 were used to further probe the fibre data, leading to the following conclusions:

- It is possible to determine whether the tunnel is heaving or settling from the transverse fibre optic data and, in fact, the fibre strain profile during heave is simply an inverted profile of the fibre strain profile during settling.
- The fibres are able to identify the point at which the heaved soil starts to settle, and the fibre data suggests a change in the shape of the settlement profile when compared to the heave profile.
- The fibre data indicates the direction of rotation of the cutterhead.

- In the longitudinal direction the fibre strain profile is again dominated by horizontal strains.

Further Research

It is proposed to run further tests using fibre optic cables to measure strains in the TBM rig, and to combine this data with results from LVDTs – or another technique for obtaining surface settlements – to further explore the relationship between the fibre strain profile and the obtained settlement/heave profiles.

4.6 Can a comparison with tunnelling illuminate the process?

In order to determine the similarities between the plane strain trapdoor rig and tunnelling, the same techniques published in literature to analyse tunnelling are applied to the data from the trapdoor tests. This has already been shown in part in Section 4.4.1, with the gaussian fits commonly used for tunnelling, applied to the trapdoor rig settlements.

This can be further extended by exploring the factor K, as defined in Equation 1. In order to investigate the behaviour of K with depth, Equation 1 can be modified to give:

$$i_x = K(z - z_0) \tag{14}$$

This allows K to be tracked with height; and by combining Tests 2 and 3 with some of Della Ragione's (2020) tests (Table 5), with relative density (Figure 37). Comparing this with results

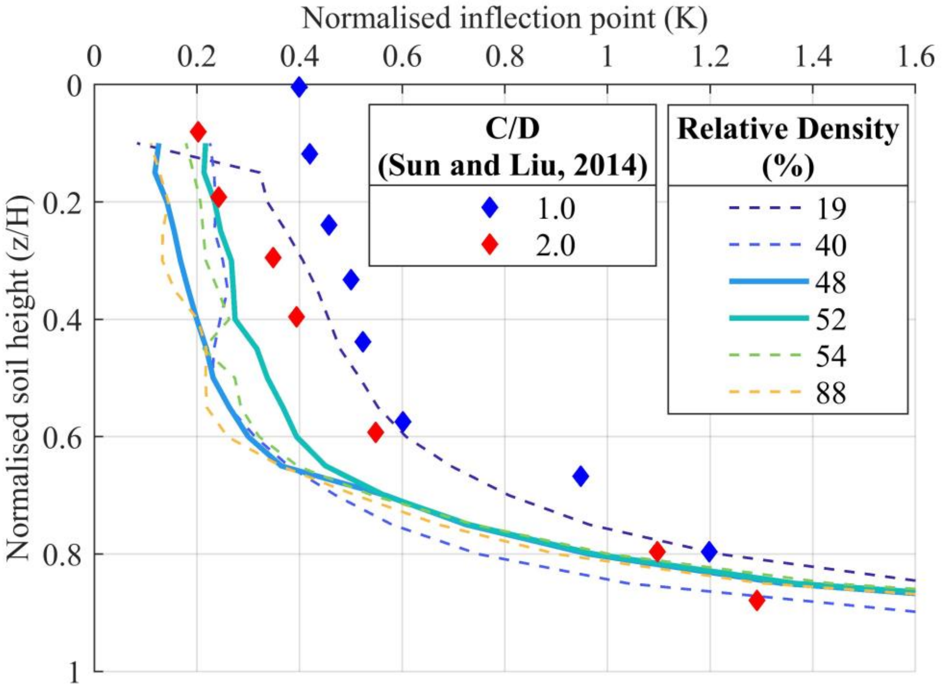

Figure 37: Normalised inflection point with soil height for Tests 2 and 3 (solid lines); and four of Della Ragione's (2020) tests (dashed lines); compared with results from Sun and Liu (2014).

published in literature (also shown in Figure 37) it is clear that the behaviour in the trapdoor tests is comparable. Sun and Liu (2014) performed their experiments by manually retracting a glass bar from a model in order to trigger soil movement. There are two trends in Figure 37 for different cover to diameter ratios. For the trapdoor tests performed this ratio was 2. Hence, comparing the sinkhole data to the trend for the same ratio, both show K of around 0.2 at the surface and have a decaying shape. This further confirms that the behaviour of the two processes is very similar.

It is also possible to look at the behaviour of the factor k from Equation 12, relating the horizontal to the vertical soil displacements. This factor can be re-expressed as:

$$k = \frac{1}{\left(\frac{z_f}{z_0}\right)} \tag{15}$$

where z_f is the depth of the soil displacement vector focus (Figure 38). The behaviour of this factor can be plotted across the depth of the sample and with different relative densities (Figure 39(a)). This clearly shows a consistent trend and hence it is possible to compare this trend to those found in literature. By comparing an enlarged version of Figure 39(a) with predictions made using finite element analysis (FEM) (Losacco and Viggiani, 2019) for tunnelling in clays (Figure 39(b)) it is apparent that at shallower depths the PIV data matches the FEM predictions very well. As the depth is increased the factor no longer follows the linear trend and instead increases exponentially. This is expected, as the displacement vector foci are known to be located considerably deeper in sands than in clays. The similarity in the trends further reinforces that the plane strain trapdoor exhibits similar behaviour to the tunnelling process.

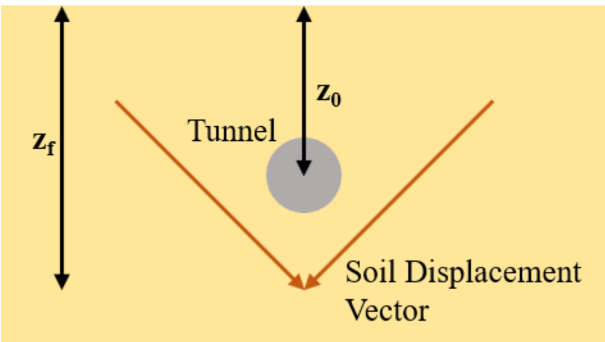

Figure 38: Soil displacement vectors.

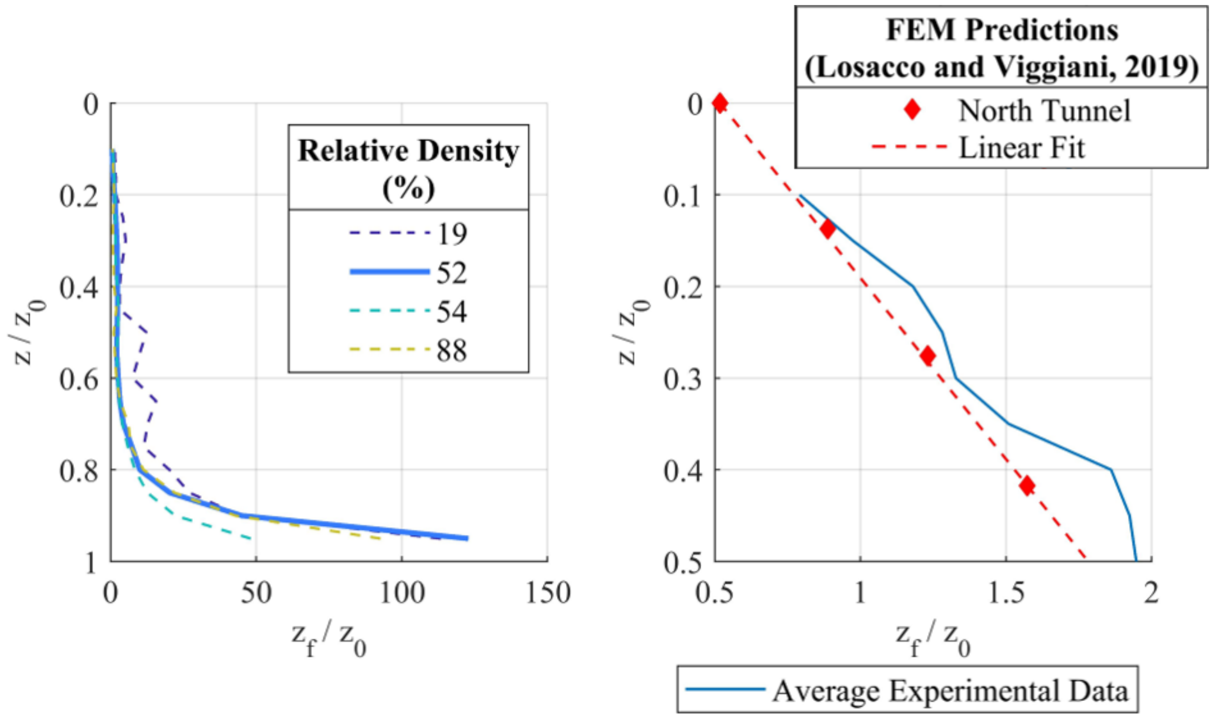

(a) *(b)*

Figure 39: z_f / z_0 with depth (a); and an enlarged version comparing the data to predictions used in tunnelling (b) (Losacco and Viggiani, 2019).

It is also possible to compare the fibre optic data obtained in both tests. This was touched upon in Section 4.5.1 and will be further explored here. When comparing the two profiles (Figure 40) it is immediately apparent that both have a similar shape and share similar characteristics. This comparison is only possible towards the end of Test 4, as initially the heave led to an inverted fibre profile. However, the settlement that was experienced after the heave, gives rise to a strain profile which is similar to that obtained in the trapdoor tests. The key difference in the two profiles, when exploring the shape, is that the tunnelling strain profile is considerably wider than the trapdoor strain profile, with the peak strains occurring at a dimensionless distance of 2.5 compared to 1.5. This is due to the fact that the trapdoor rig exhibits a chimney mechanism with steep soil settlements whereas the TBM rig exhibits a more conical trend in settlement profile widths, and hence the profiles are wider on the TBM rig.

The other natural comparison between the two profiles is to compare the strain magnitudes. For the tunnelling test the magnitudes have been tracked as the tunnel travels past the fibre (Figure 41) and for the fibre they have been tracked for small trapdoor displacements (Figure 42). The strains are of the same order of magnitude and enable a direct comparison between the results. It is important to note once again that for the TBM test the soil was heaving initially and hence the results from the end of the test are of particular interest. At the end of the tunnelling test the

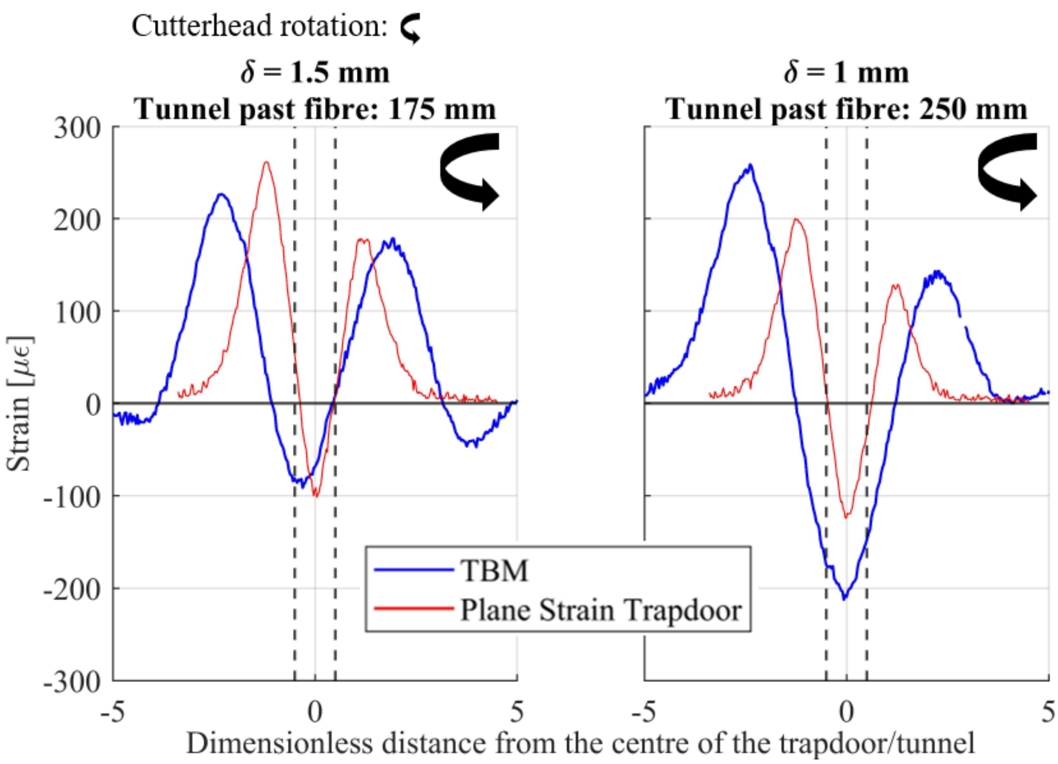

Figure 40: Fibre strain profiles obtained from the TBM rig (Test 4) and the plane strain trapdoor rig (Test 3).

strain magnitude of around 250 με is very similar to the strain magnitude for a trapdoor displacement of 2 mm. Due to the lack of LVDT data it is not possible to perform a volume loss comparison across the two, but in future tests it is recommended to attempt this in order to

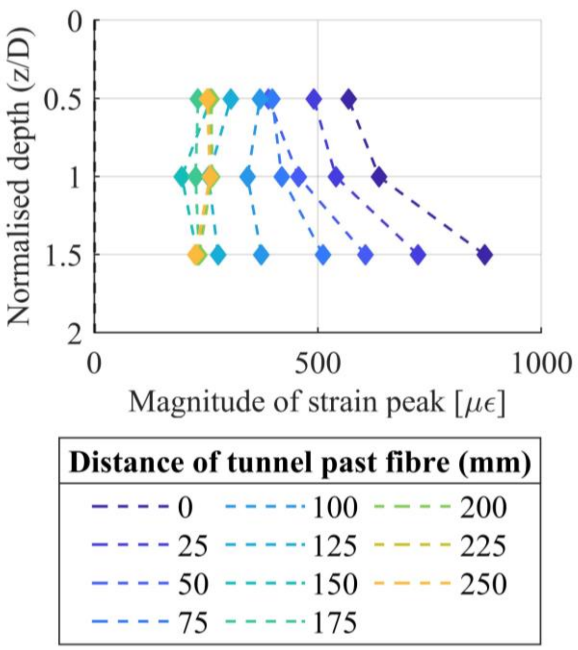

Figure 41: Peak strain magnitudes with depth, as the tunnel progresses beyond the fibre, for Test 4.

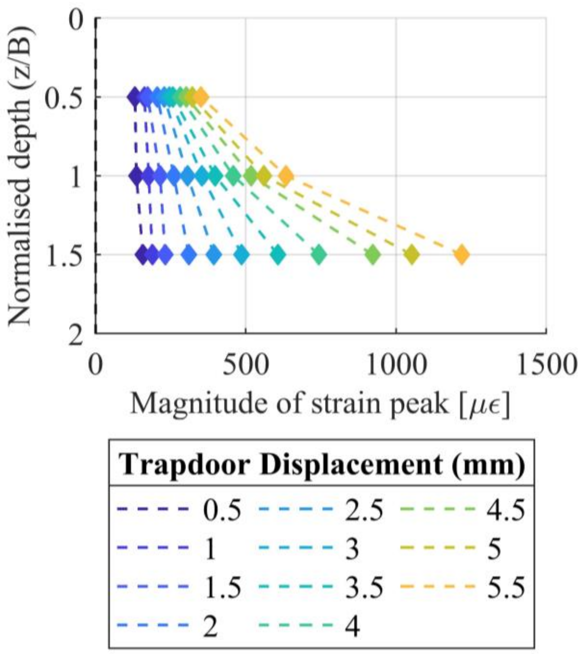

Figure 42: Peak strain magnitudes with depth, as the trapdoor displacement increases, for Test 3.

determine whether the two strain magnitudes are comparable when the volume loss is the same.

Summary

Data from the plane strain trapdoor rig has been compared with literature on tunnelling. The fibre data from both rigs has also been compared, leading to the following conclusions:

- There are very strong similarities between the plane strain trapdoor rig and tunnelling which can be exploited for analysis of the data and transferring knowledge of experimental techniques.
- These can be quantified both by comparing PIV results to literature and directly comparing the fibre data across the two rigs.
- The strain profiles obtained in both tests are very similar for the times when both are settling, although the profile width for the TBM test was larger due to the differences in soil behaviour.
- The strain magnitudes are very similar.

Further Research

It is suggested to perform a further set of comparable tests in the plane strain trapdoor and the TBM rig, ensuring that the soil is settling, and that surface settlement data is acquired in the TBM rig. For instance, a raspberry pi camera setup could be used to capture surface deformations and enable surface reconstruction. This would allow for a more direct comparison of the two tests.

5 Conclusions

5.1 Project Contributions

1g tests were performed in a 2D plane strain trapdoor rig in order to explore the geomechanics of sinkhole formation. Fibre optic cables were placed into the sand to determine whether these are capable of locating and measuring ground deformations.

A range of fibre optic laying techniques were explored. Firstly, it was demonstrated that coupling between the fibres and the surrounding soil is a critical factor and this can be improved by increasing the interface roughness of the fibre. Secondly, it was shown that the fibre strain profile fits within the confines of the rig and hence the fixing method used at the edges does not influence the data. Thirdly, it was discovered that introducing slack into the fibres improves their ability to follow the soil deformations. However, this does impact the ease of mapping points on the fibre to locations within the soil. These results inform on potential techniques for laying fibres in future laboratory and field tests.

PIV was used to explore the behaviour of the soil, and this data was compared to the fibre data. In order to facilitate this, the PIV system was updated from a calibration marker-based system to a CharuCo board system. This improved the quality of the data and removed some data losses. It was observed, upon comparison with the PIV data, that the fibre optic data clearly contains a signature strain profile which is comparable to the horizontal strains calculated using the PIV data. This reinforces the proposal of using DFOS as an early warning system for sinkholes. Secondly, it was noted that the fibre profile width is wider than the width of the soil settlements. This demonstrates that DFOS is a conservative method for sizing sinkholes. It is suggested to combine DFOS monitoring with GPR in order to accurately determine the size and depth of a sinkhole once the DFOS has identified its location.

1g tests were also performed on a TBM rig in order to explore the behaviour of the fibre optic cables under different conditions. It was apparent from the fibre data whether the ground was heaving or settling. The fibres are even able to identify when heaved soil begins to settle and can track changes in shape of the settlement profile. It was also possible to determine the direction of the cutterhead from the fibre data. As noted in the plane strain trapdoor tests, it was once again apparent that the strain profile obtained from the fibre is dominated by the horizontal strain in the soil. All of this reinforces the usefulness of fibre optic cables for measuring ground displacements in geotechnical engineering.

Finally, data from the trapdoor rig was compared with literature on tunnelling and the fibre data from both rigs were compared with each other. It was concluded that there are strong similarities between the plane strain trapdoor rig and tunnelling indicating that analysis techniques used for tunnelling can be applied to the sinkhole formation process.

5.2 Future Work and Recommendations

In order to continue developing an early warning system for sinkholes many other factors need to be considered. One of these is saturation, which could be explored by running laboratory tests in saturated sand. This would enable exploration of the impact that cohesion has on the formation process and the behaviour of the fibre.

More specifically to HS2, factors such as geosynthetics should be explored as railway embankments often incorporate these in order to stabilise the soil. This not only affects the sinkhole formation behaviour, but it also presents an opportunity for weaving the fibre optic cable through the geosynthetic, thereby considerably changing the behaviour of the fibre. The effect of the embankment itself in terms of the overburden pressure and the shape should also be investigated. This could be achieved using an embankment placed on the surface of a model. Stress levels in the field could be more accurately simulated by running centrifuge experiments.

Other future considerations include the effect of layered soils which could be investigated both in the field and in laboratory tests. In particular, the build-up of railway embankments should be explored, running tests on models containing the ballast, sub-ballast, blanket, and subgrade typical of UK railway routes. Finally, another key consideration to explore is the effect of the earthworks likely to be used when laying the fibre optic cables, as this will impact the laying techniques employed. This could be achieved by running full scale field tests.

Concluding Remarks

The objectives of this project were threefold: to explore the fibre laying process; to improve the understanding of the DFOS data; and to compare the sinkhole formation process to tunnelling. Within the tests conducted, different techniques for laying fibres were explored and recommendations for future fibre laying were made. The DFOS data was compared to PIV data and these observations enabled several important conclusions about the DFOS data to be made. Finally, a comparison with literature, and between tests, clearly indicated that there are significant similarities between the two processes and that the same analysis techniques can be used for both.

6 References

Al-Naddaf, Mahdi, Jie Han, Saif Jawad, and Ghaith Abdulrasool. 2017. "Investigation of Stability of Soil Arching under Surface Loading using Trapdoor Model Tests."

Alrowaimi, Mohamed, Hae-Bum Yun, and Manoj Chopra. 2015. "Sinkhole Physical Models to Simulate and Investigate Sinkhole Collapses."

Bolton, M. D. 1986. "The strength and dilatancy of sands." *Géotechnique* Volume 36, Pages 65-78.

Chang, Ling, and Ramon F. Hanssen. 2014. "Detection of cavity migration and sinkhole risk using radar interferometric time series." *Remote Sensing of Environment* Volume 147, Pages 56-64.

Costa, Yuri D., G. Jorge Zornberg, Benedito S. Bueno, and Carina L. Costa. 2009. "Failure Mechanisms in Sand over a Deep Active Trapdoor." *Journal of Geotechnical and Geoenvironmental Engineering* Volume 135.

da Silva, Talia Simone. 2017. *Centrifuge Modelling of the Behaviour of Geosynthetic-Reinforced Soils above Voids.* Cambridge: University of Cambridge.

Della Ragione, Gianluigi. 2019-2020. Informal communication and presentations.

Della Ragione, Gianluigi. 2020. "Experimental and Numerical Study on the Use of Distributed Fibre Optic Sensing Techniques as Early Warning System for Sinkhole Detection."

Fargnoli, V., D. Boldini, and A. Amorosi. 2013. "TBM tunnelling-induced settlements in coarse-grained soils: The case of the new Milan underground line 5." *Tunnelling and Underground Space Technology* Volume 38, Pages 336-347.

Glossop, Nigel H. 1978. *Soil deformations caused by soft-ground tunnelling.* Durham: Durham University.

Iglesia, Geraldo R., Herbert H. Einstein, and Robert V. Whitman. 2014. "Investigation of Soil Arching with Centrifuge Tests." *Journal of Geotechnical and Geoenvironmental Engineering* Volume 140, Pages 04013005.

Jacobsz, S. W. 2015. "Trapdoor Experiments Studying Cavity Propagation." *Proceedings of the First Southern African Geotechnical Conference.* Pages 159-165.

Jennings, J. E., A. B.A. Brink, A. Louw, and G. D. Gowan. 1965. "Sinkholes and Subsidences in the Transvaal Dolomite of South Africa."

Jennings, J. N. 1971. *An Introduction to Systematic Geomorphology - Volume Seven - Karst.*

Kechavarzi, Cedric. 2016. *Distributed fibre optic strain sensing for monitoring civil infrastructure: a practical guide.* London: ICE Publishing.

Klar, Assaf, Idan Dromy, and Raphael Linker. 2014. "Monitoring tunnelling induced ground displacements using distributed fiber-optic sensing." *Tunnelling and Underground Space Technology* Volume 40, Pages 141-150.

Labuschagne, J., M. Ferentinou, M. Grobler, and S. W. Jacobsz. 2019. "Smart Monitoring of Sinkhole Formation Using Optic Fibre Technology." *Information Technology in Geo-Engineering, Proceedings of the 3rd International Conference (ICITG).* Guimarães. Pages 763-773.

Losacco, Nunzio, and Giulia M.B. Viggiani. 2019. "Class A prediction of mechanised tunnelling in Rome." *Tunnelling and Underground Space Technology* Volume 87, Pages 160-173.

Madabhushi, S. P.G., N. E. Houghton, and S. K. Haigh. 2006. “A new automatic sand pourer for model preparation at University of Cambridge.” In *Physical Modelling in Geotechnics*, by C. W.W. Ng, Y. H. Wang and L. M. Zhang, Pages 217-222.

Mair, R. J. 2008. “Tunnelling and geotechnics: new horizons.” *Géotechnique* Volume 58, Issue 9, Pages 695-736.

Marshall, A. M., R. Farrell, A. Klar, and R. Mair. 2012. “Tunnels in sands: the effect of size, depth and volume loss on greenfield displacements.” *Géotechnique* Volume 62, No. 5, Pages 385-399.

Meguid, M. A., O. Saada, M. A. Nunes, and J. Mattar. 2008. “Physical modeling of tunnels in soft ground: A review.” *Tunnelling and Underground Space Technology* Volume 23, Issue 2, Pages 185-198.

O'Reilly, Myles, and Barry New. 1982. “Settlements above tunnels in the United Kingdom - their magnitude and prediction.”

Rawal, Kishor. 2016. *Exploring the Geomechanics of Sinkholes: A Preliminary Numerical Study*. The University of Toledo.

Selby, A. R. 1999. “Tunnelling in soils - ground movements, and damage to buildings in Workington, UK.” *Geotechnical and Geological Engineering* Volume 17, Pages 351-371.

Soliman, Moataz H., Adam L. Perez, Boo Hyun Nam, and Ming Ye. 2018. “Physical and Numerical Analysis on the Mechanical Behaviour of Cover-Collapse Sinkholes in Central Florida.” *15th Multidisciplinary Conference on Sinkholes and the Engineering and Environmental Impacts of Karst.* Sheperdstown.

Stanier, S. A., J. Blaber, W. A. Take, and D. J. White. 2015. “Improved image-based deformation measurement for geotechnical applications.” *Canadian Geotechnical Journal* Volume 53, Pages 727-739.

Sun, Jizhu, and Jinyuan Liu. 2014. “Visualisation of tunnelling-induced ground movement in transparent sand.” *Tunnelling and Underground Space Technology* Volume 40, Pages 236-240.

Terzaghi, K. 1936. *Stress Distribution in Dry and in Saturated Sand above a Yielding Trapdoor*.

Tien. 1996. “Relevance and Application of Arching in Geotechnical Engineering.” Pages 27-39.

Vorster, T. E.B., Assaf Klar, Kenichi Soga, and R. J. Mair. 2005. “Estimating the Effects of Tunnelling on Existing Pipelines.” *Journal of Geotechnical and Geoenvironmental Engineering* Volume 131, Pages 1399-1410.

Zhang, Cheng-Cheng, Hong-Hu Zhu, and Bin Shi. 2016. “Role of the Interface between Distributed Fibre Optic Strain Sensor and Soil in Ground Deformation Measurement.” *Scientific Reports* Volume 6, Pages 36469.

Zhao, Y, K Gafar, M. Z.E.B. Elshafie, A. D. Deeks, J. A. Knappett, and S. P.G. Madabhushi. 2006. “Calibration and use of a new automatic sand pourer.” In *Physical Modelling in Geotechnics*, by C. W.W. Ng, Y. H. Wang and L. M. Zhang, Pages 265-270.

7 Appendices

7.1 Appendix 1: Risk Assessment Retrospective

The risk assessment submitted in October 2019 outlined electrical risks associated with operating the experimental setup, mechanical risks associated with operating the trapdoor control mechanism and physical risks due to hydraulic pistons, although these were not pressurised. The risks posed by dust due to working with sand and manual handling risks were also outlined. This was followed by an extended risk assessment outlining control measures undertaken to minimise these risks and quantifying the remaining risk level. The actions undertaken were successful and the remaining risk levels were accurately predicted.

There was however one risk which was not predicted in advance. The use of hazardous substances was not highlighted as a potential risk, but hazardous substances were used, both to clean the rig and also to setup the tests. Appropriate action was taken by following the guidelines of the Schofield Centre on handling such chemicals, and no problems ensued.

In future, it would be beneficial to consider unexpected risks by exploring the risks commonly found in the Schofield Centre and assuming that it is likely that any project in the Schofield Centre will face similar risks, even when this is not necessarily clear from the outset.

7.2 Appendix 2: Covid-19 Appendix

Due to circumstances beyond the author's control the LVDT data from the TBM test (Test 4) was not available which has influenced the data analysis. The loss of the LVDT data was discovered at the beginning of April and ideally a repeat of this test would have been performed at the end of April after the exams. However, due to the Covid-19 lockdown it was not possible to perform a second run of the TBM test.

As the title of this project concerns the comparison of the sinkhole formation process and tunnelling, the author felt that it was not possible to ignore Test 4 and that this issue could not be avoided by redefining elements of the project. Instead, it was attempted to analyse the data from the TBM test as best as possible. This was achieved by incorporating data from literature and also data from a similar test performed by Casey Shepheard (a PhD student in the Schofield Centre).

Although this analysis was successfully performed, and several conclusions were dawn it is clear that some of the intended comparisons have been left as future research as it is simply not possible to answer these questions without the missing data.